Behaviour of Partially Earth-anchored Cable-stayed Bridge with Crossing Cables of Different Side-to-Main Span Ratios

Motasem AlSayed

A Thesis

in

The Department

of

Building, Civil and Environmental Engineering

Presented in Partial Fulfillment of the Requirements

for the Degree of Master of Applied Science (Civil Engineering) at

Concordia University

Montreal, Quebec, Canada

November 2019

CONCORDIA UNIVERSITY

School of Graduate Studies

This is to certify that the thesis prepared

By: Motasem AlSayed

Entitled: Behaviour of Partially Earth-anchored Cable-stayed Bridge with Crossing Cables of Different Side-to-Main Span Ratios

and submitted in partial fulfillment of the requirements for the degree of

Master of Applied Science (Civil Engineering)

complies with the regulations of the University and meets the accepted standards with respect to originality and quality.

Signed by the final examining committee:

_____ Dr. M. Nik-Bakht	Chair, Examiner
_____ Dr. V. S. Hoa	Examiner
_____ Dr. E. Erkmen	Examiner
_____ Dr. L. Lin	Supervisor
_____ Dr. J. Hassan	Supervisor

Approved by _____

Chair of Department or Graduate Program Director

November 2019 _____

Dean of Faculty

ABSTRACT

Behaviour of Partially Earth-anchored Cable-stayed Bridge with Crossing Cables of Different Side-to-Main Span Ratios

Motasem AlSayed

Maximising the main span length of cable-stayed bridges while optimizing the cost of construction is a bridge engineering challenge. One solution has been suggested by Shao et al. (2014) who proposed a partially-earth anchored system in conjunction with crossing cables at the main span as a new system for cable-stayed bridges. The main span length tested in their study was 1408 meters, which is much longer than existing conventionally constructed bridges. Although analysis results demonstrated that the proposed system has advantages over conventional systems, it is still under development and has not been adopted in practice.

The purpose of this study therefore is to evaluate the structural response of a cable-stayed bridge under the proposed new system of different side-to-main span ratios. The bridge considered in Shao et al. (2014) is used for analysis. Six side-to-main span ratios, i.e., 0.24, 0.27, 0.30, 0.33, 0.36 and 0.39, are tested. Three-dimensional finite element models are developed using structural analysis software SAP2000. The models are subjected to dead load, traffic load, and earthquake load to test the response of the bridge's superstructure and substructure.

From this study it is found that under static loads the side-to-main span ratios have a significant effect on girder axial force and anchorage, while having a very minor effect on cables. The results also show that the ratio does not affect the bending moment of the main span, but that when a small ratio is considered particular attention needs to be paid to the pier farther from pylon to avoid uplifting. Deck vibration and longitudinal movement, as well as pylon lateral displacement, would not be an issue for this super-long bridge. However, it might be necessary to take appropriate action to allay concerns over residual displacement due to earthquake load.

ACKNOWLEDGEMENTS

I would like to present my sincere thank you to Dr. Lin, L. as well as Dr. Hassan, J. who were present to provide assistance throughout my study with their efforts and guidance. Dr. Lin's knowledge in bridge engineering and her research experience were essential to the work. The time she dedicated was crucial in furthering my work. Dr. Hassan was constantly present with constructive criticism, comments and suggestions which were all sincerely appreciated. Dr. Lin along with Dr. Jassim made this work possible and so I am extremely thankful.

Most importantly, I would like to dedicate my thesis to my beloved older sister Hadeel. She was present through all my ups and downs. While she is no longer amongst us, her support made me the person I am. Having been away from my family for the length of my program was not an easy task for either of us but they kept encouraging me to succeed. I want to mention the appreciation and gratitude to my mother, father, and two younger sisters Dania and Tala for their ongoing trust and patience during this time. While I wish I could have been present for my late sister and my younger sisters, I owe them nothing but thanks in my achievements.

I am grateful to everyone who was there from the beginning to the end.

Colleagues and friends and everyone in between, thank you.

TABLE OF CONTENTS

LIST OF FIGURES

LIST OF TABLES

CHAPTER 1

INTRODUCTION

1.1 General

Super-long span bridges are typically represented by cable-stayed bridges and suspension bridges. The difference between the two systems can be visualized if the cables are placed with an inclination (cable-stayed bridge) or they are placed straight vertically (suspension bridge). In a cable-stayed bridge system, these cables not only provide intermediate supports to the deck but also transfer the load to the pylon and anchorages at the ends of the bridge. Eventually, all the loads are transferred to foundation.

Considering the material strength and the total cost, both researchers and industry practitioners have proposed the maximum economical span length for suspension bridges and cable-stayed bridges. In the past, it was well accepted the maximum span length for a cable-stayed bridge system was about 1000 m as shown in Svensson (2012). Beyond this length, it is favourable to consider the suspension bridge system. However, with the improvement of knowledge about cable-stayed bridges and the advancing of construction technology, the span length of several cable-stayed bridges has exceeded the limit of 1000 m. The recent completed Russky Bridge in Russia in 2012 has the span length of 1104 m, Sutong Bridge in China completed in 2008 has the span length of 1088 m. It is reported that the span length of Changtai Yangtze River Bridge in China to be completed in 2024 will reach about 1200 m. On the other hand, as the span length of the cable-stayed bridge increases, firstly, extensive compression force is expected to be developed in the girder. Accordingly, larger section dimension has to

be considered for members, which in turn will add more loads to the substructure. Secondly, the height of the tower needs to be increased in order to accommodate more cables to reduce the axial force in the girder. They both will ultimately increase the total cost of the bridge.

Recently, Shao et al. (2014) proposed a new system called partially earth-anchored system in conjunction with the use of crossing cables at the main span for cable-stayed bridges. Research results have shown that this new system would save the total cost of the bridge by about 12% compared to the conventional system currently considered by designers. Although it has been approved that this new system has advantages over the old ones, the system development is still at early stage. In particular, the side-to-main span ratio of 0.39 considered in Shao et al. (2014) is reported to be the optimal ratio for the self-anchored system by Gimsing and Georgakis (2012). Given this, comprehensive research is required to study the performance of cable-stayed bridges with the new system in order to optimize the design, maximize the span length without compromising the cost, and develop durable construction technology to speed up construction.

1.2 Objective of the Study

The objective of this study is to examine the effects of side-to-main span ratio on the response of a cable-stayed bridge using partially earth-anchored system in conjunction with crossing cables at its main span. To achieve this objective, the following tasks are followed:

- Develop a 3D finite element model of the bridge under examination using SAP2000,
- Validate the model based on the results available in literature,
- Evaluate performance of the bridge under static loads, such as, dead load and traffic load, and
- Investigate dynamic response of the bridge under earthquake load.

1.3 Outline of the Thesis

This thesis is organized into five chapters including this chapter.

Chapter 2 reviews principles for each of the three existing anchorage systems. It also summarizes previous studies on cable-stayed bridge structural system in line with the objective of this study.

Chapter 3 describes the bridge to be examined in this study. Finite element modelling of the bridge is explained in detail. Modal validation is discussed at the end of the chapter.

Chapter 4 presents results on both superstructure and substructure due to three loads, i.e., dead load, traffic load and earthquake load from the analysis on the bridge model. Six side-to-main span ratios, i.e., 0.24, 0.27, 0.30, 0.33, 0.36 and 0.39, are used for the analysis.

Chapter 5 summarizes the main findings and conclusions from this study. Recommendation for future research work is also provided in this chapter.

CHAPTER 2

LITERATURE REVIEW

2.1 Cable System Anchorage

Cable-stayed bridge system can be classified as a fan system, a semi-fan system or a harp system as illustrated in Fig. 2.1 depending on the arrangement of cables along the pylon. In particular, in a fan system all the cables are attached to a single point on the pylon, which is the top of the pylon in almost of the cases; in a semi-fan system the cables are attached to multiple points along the upper part of the pylon and the inclined angle of each cable is different; in a harp system, the cables are anchored along the entire height of the pylon and the cables are nearly parallel as shown in Fig. 2.1.

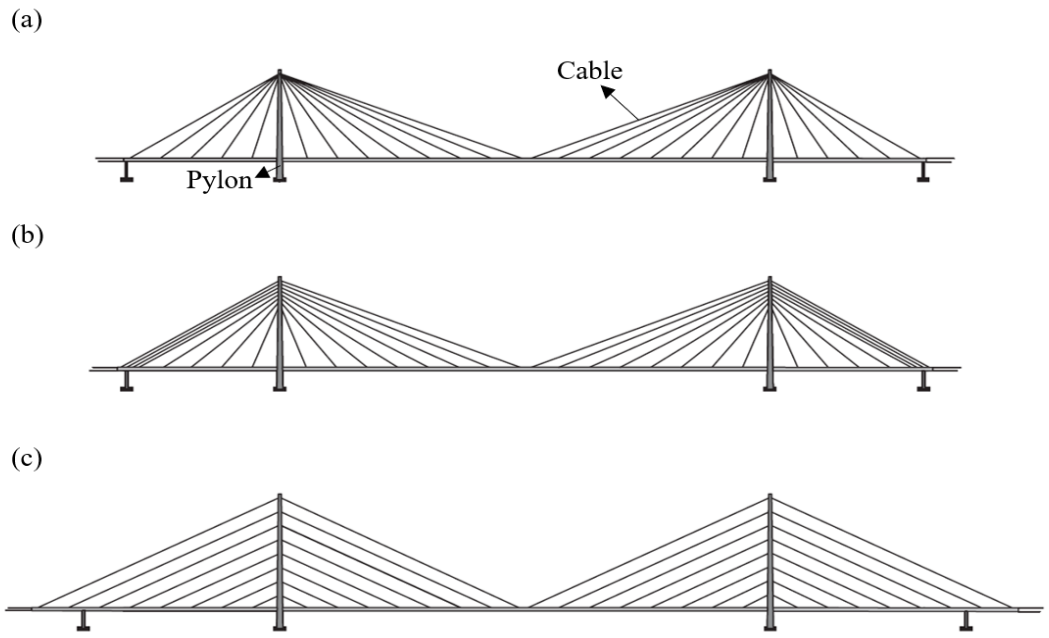

Figure 2.1 Cable-stayed bridge systems: (a) fan system, (b) semi-fan system, and (c) harp system as Gimsing and Georgakis (2012).

It was reported by Tang (2000) that the fan system is suitable only for a limited number of cables and the harp system is not economical and efficient for longer spans. Though the harp system gives a pleasant appearance compared with the other two systems, the pylon must be tall enough and must be designed with larger cross sections to achieve sufficient stiffness. It can be seen in Fig. 2.1 that the configuration of the semi-fan system is a cross between the fan system and the harp system. The main advantages of the semi-fan system are, (i) cables are attached to multiple points along the pylon to avoid the anchorage difficulties encountered in the construction of the fan system, (ii) larger axial forces developed in the harp system are reduced by using steeper cables while the pleasant appearance of the bridge is maintained (Svensson, 2012; Gimsing and Georgakis, 2012; Leonhardt, 1987). Given this, the semi-fan system is commonly used in the construction of the modern cable-stayed bridges, such as, 890 m-long Tatara Bridge, 1088 m-long Sutong Bridge, 1104 m-long Russky Island Bridge.

A cable-stayed bridge can also be considered as an earth-anchored bridge, self-anchored bridge or a partially earth-anchored bridge based on how the side span is anchored. A detailed description of each system is given below.

2.1.1 Earth-anchored system

In the earth-anchored system, each span is simply supported. As illustrated in Fig. 2.2, a fixed bearing is used at the end support of each side span to restrict the horizontal movement of the deck, and expansion bearings are used at the middle span to allow the translation of the deck in the bridge longitudinal direction. Accordingly, cables do not generate compressive horizontal forces in the deck, but rather large tensile force at the middle of the main span.

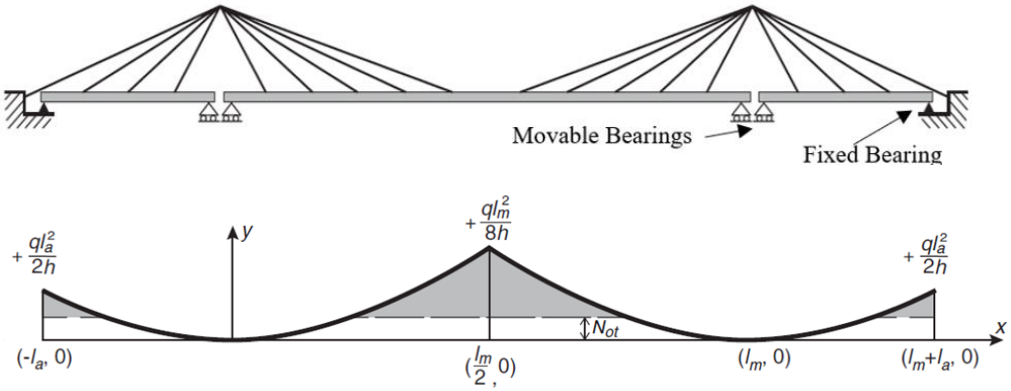

Figure 2.2 Layout and schematic axial force diagram of the earth-anchored system as Gimsing and Georgakis (2012).

At the side span, the horizonal and the vertical components of force in cables are not transferred to the deck, but are taken by the earth anchor (Fig. 2.3).

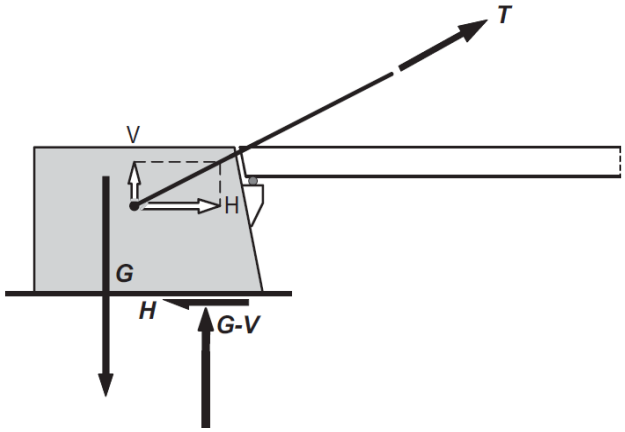

Figure 2.3 Mechanics at connection between anchor cable and anchor block in an earth-anchored system as Gimsing and Georgakis (2012).

2.1.2 Self-anchored system

In the self-anchored system, the deck is continuous along the entire bridge, movable bearings are used at the both ends of the bridge (Fig. 2.4), and all the cables are attached to the deck. For comparison purpose, Figure 2.5 present mechanics at the anchorage block at the bridge end.

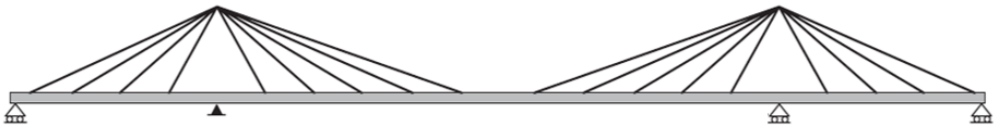

Figure 2.4 Layout of self-anchored system as Gimsing and Georgakis (2012).

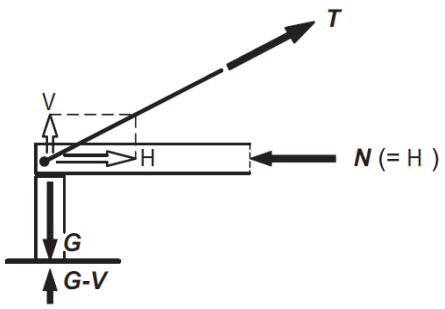

Figure 2.5 Mechanics at connection between anchor cable and anchor block in a self-anchored system as Gimsing and Georgakis (2012).

In this system, the deck along the entire bridge is subjected to compression. The vertical component of the cable force is transferred to the Pylon. As an example, Figure 2.6 shows the axial force distribution in the deck in the main span in which the force is quite small near the middle of the span while it is accumulated to the maximum around the location of the pylons. By using the self-anchored system designers have been able to expand the main span length of cable-stayed bridges from 180m (Stromsund Bridge, completed in 1955) to 1104 m (Russky Island Bridge, completed in 2012), i.e., the span is increased almost 7 times. However, Gimsing and Georgakis (2012) raised a concern on the use of the self-anchored system with a main span exceeding 1500 m. They reported that the compression force in the deck might become significant with the increase of the span length. Especially, the design of the deck will be governed by dead load if the span length is beyond a certain limit. Their finding is consistent with the one given in Tang (2000).

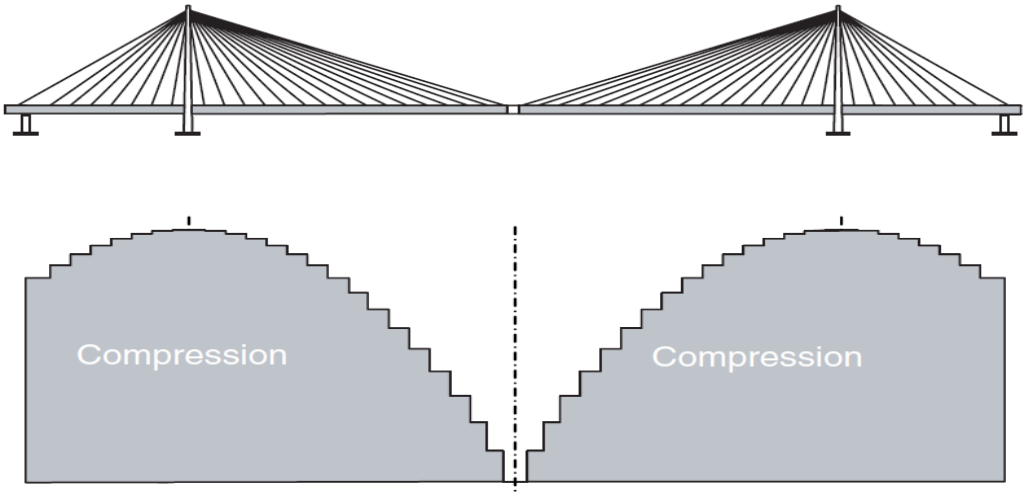

Figure 2.6 Diagram of axial force in the deck at the main and side span in a self-anchored system as Gimsing and Georgakis (2012).

2.1.3 Partially earth-anchored system

In the partially earth-anchored system (Fig. 2.7), the deck is also continuous along the entire bridge like the self-anchored system. However, the deck sits on movable bearings. Most of the cables are attached to the deck while the anchoring cables are directly connected to the anchor

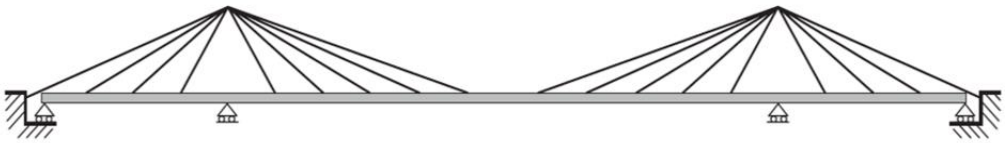

Figure 2.7 Layout of partially earth-anchored system as Gimsing and Georgakis (2012).

block. Figure 2.8 demonstrates a deck axial force diagram of a 3-span bridge using partially earth-anchored system. In the equations for determination the axial force at three typical points (two pylon locations, and middle of main span), L_s is the side span length, L_m is the main span length, h is the height of the pylon above the deck, and q is the uniform dead load applied on the deck due to self-weight of the deck.

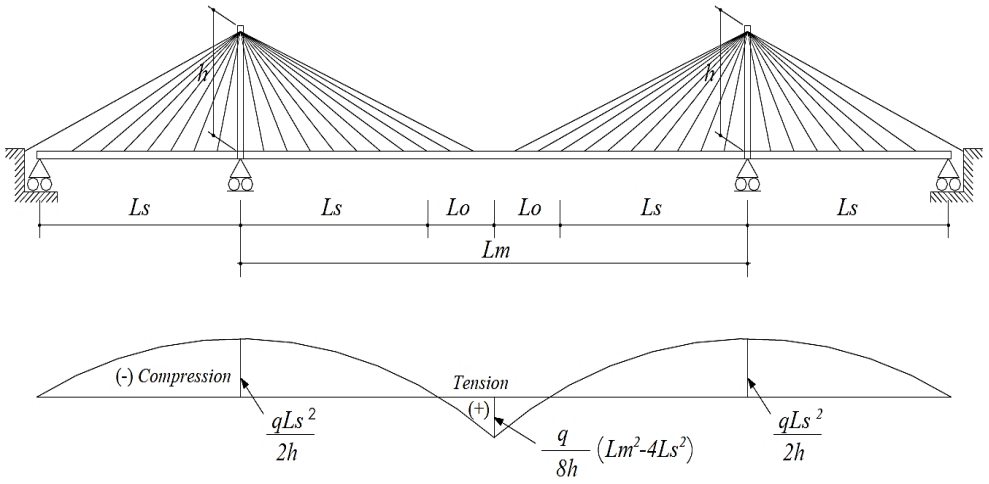

Figure 2.8 Diagram of axial force in the deck in a partially earth-anchored system (Kim and Won, 2016).

By comparing Fig. 2.8 with Fig. 2.6, it can be seen clearly the effect of the anchorage system on the axial force in the deck, i.e., tension forces are developed in the main span in the partially earth-anchored system. These forces, in turn, reduce the maximum compressive force in the deck at the sections close to the pylon. This indicates the advantage and efficiency of the partially earth-anchored system, namely, the lower compressive force the smaller deck section. Such tendency will eventually lead to a longer span length as discussed in Nagai et al. (2004), Sun et al. (2010) and Jin et al. (2016).

2.2 Past Studies on Improving the Bridge Structural System

2.2.1 Studies conducted before 2000

The concept of the partially earth-anchored cable-stayed bridge was originally developed by Gimsing around 1980s to reduce the significant compressive force in the deck observed in the self-anchored system. Couple of years later, Otsuka et al. (1990) proposed a partially anchored composite cable-stayed bridge, in which the middle span was made of steel while all the other spans were made of prestressed concrete. In order to improve the performance of self-anchored system and earth-anchored system, hinges were installed in the junction of the self-anchored girder and earth-anchored girder.

Muller (1992) proposed a bi-stayed system in order to improve bridge performance. In the bi-stayed system, the entire main span is supported by both self-anchored cables and earth-anchored cables with an equal spacing. Earth-anchored cables are anchored to anchor block; therefore, no compressive force is generated along the girder. On the other hand, internal prestress is enforced in the deck to balance the tensile force developed at the centre of the main span due to the use of the earth-anchored cables.

Starossek (1996) developed a spread-pylon cable-stayed bridge in order to decrease the peak compressive force in the main girder. Pairs of inclined pylon legs are proposed in this new system as shown in Fig. 2.9. Starossek concluded that this system would be able to reduce the height of pylons and the length of the cables. However, the system has not been adopted in practice given the inconvenience of building pylons with such a unique shape, which might significantly delay the construction.

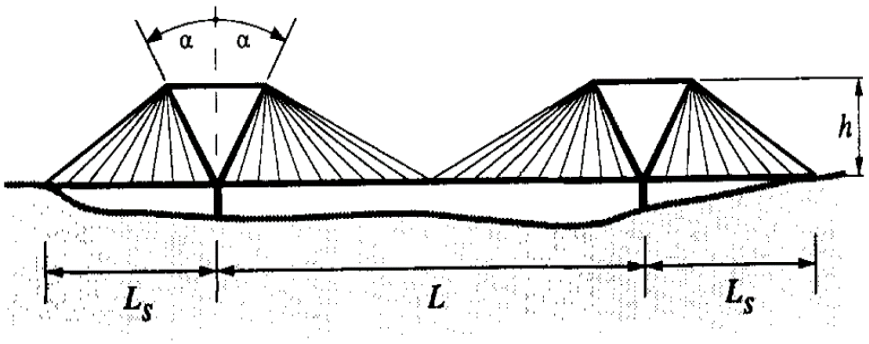

Figure 2.9 Layout of the spread-pylon cable-stayed bridge proposed in Starossek (1996).

2.2.2 Studies conducted between 2000 and 2010

In an attempt to enlarge the length of the main span of cable-stayed bridges, Nagai et al. (2004) investigated the structural performance of a 1400 m-long steel cable-stayed bridge. The effects of the span-to-girder width ratio, span-to-girder depth ratio and the thickness of the plate at the edge of the girder section on the bridge behavior were evaluated. The results of the cost analysis indicated that the span length of 1400 m was still economical for a cable-stayed bridge.

Won and Yoon (2008) examined the structural behaviour of cable-stayed bridges with partially earth-anchored system for a span length between 150 m and 500 m. Furthermore, they compared the responses of a partially earth-anchored bridge with a self-anchored system having the same geometric information. The response parameters considered for comparison were: bending moments and axial forces in the girder, vertical deflection of the girder, cable forces at the side span and main span, bending moments in the pylon, uplift forces at bearings and movements at expansion joints. They concluded that partially earth-anchored system was slightly better than self-anchored system.

Sun et al. (2010) conducted a preliminary design of a 1400 m-long cable-stayed bridge using a partially earth-anchored system shown in Fig. 2.10. In addition, Sun et al. conducted a parametric study on the bridge designed. They concluded that, (i) partially earth-anchored system is more efficient than self-anchored system at the stage when the construction is close to completion; (ii) partially earth-anchored system causes a significant decrease of axial forces in girders compared to self-anchored system, which would lead to less consumption of materials; (iii) the additional earth anchorage used in the partially earth-anchored system increases the rigidity of the bridge, and this makes the bridge less vulnerable to vibrations. More importantly, Sun et al. (2010) concluded that higher tower and smaller inclination of earth-anchored cables would be considered in construction of cable-stayed bridges.

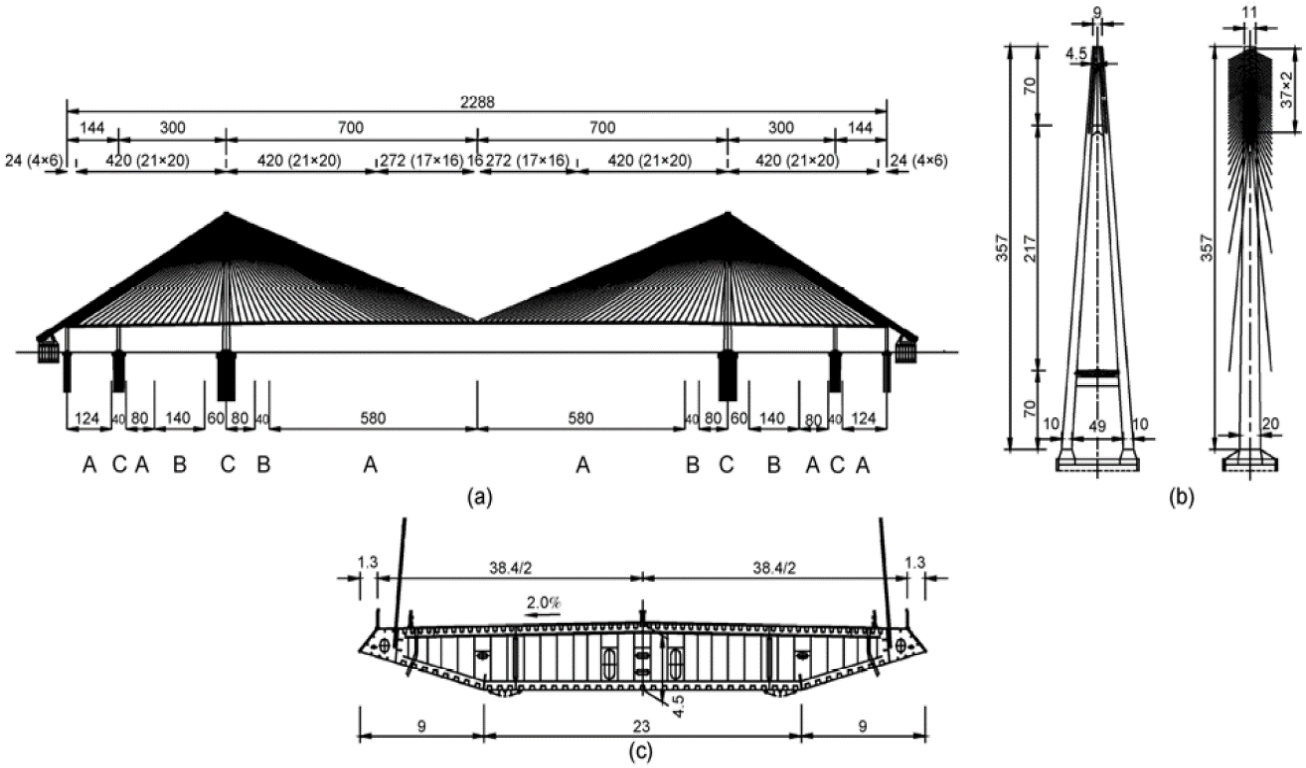

Figure 2.10 Geometric configuration of the bridge examined in Sun et al. (2010): (a) elevation view; (b) tower; (c) cross-section of girder.

2.2.3 Studies conducted after 2010

There are two major concerns in the design of cable-stayed bridges, one is excessive deflection and the other is the significant axial forces in the girder. However, the completion of the Queensferry Crossing Bridge in Scotland in 2017, which represents the biggest achievement in the history of cable-stayed bridges, demonstrates that these two issues could be resolved by using crossing cables. Figure 2.11 shows a photo of Queensferry bridge with crossing cables at the two main spans, each is 650 m long.

Figure 2.11 Photo of Queensferry Crossing Bridge, Scotland (Source: Transport Scotland).

Very recently, Shao et al. (2014) applied crossing cables to the design of a super long partially earth-anchored cable-stayed bridge in which the main span reached 1400 m (Fig. 2.12). Furthermore, they compared the axial forces in the main girder and the consumption of the materials with those where no crossing cables were used. They concluded that by using the crossing cables, the axial forces in the main girder were reduced by about 30%, and the total cost saved was around 12%. In addition, the results from their study demonstrated cable-stayed bridges can compete against suspension bridges by using both

crossing cables and partially earth-anchored system for a span length greater than 1000-1200 m, which is a typical span range dominated by suspension bridges (Gimsing and Georgakis, 2012).

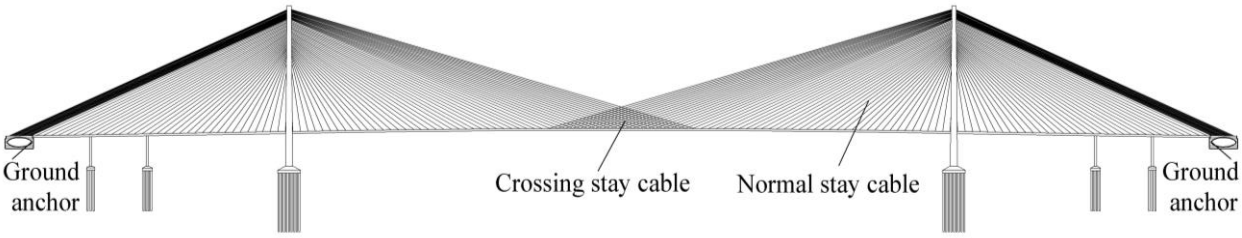

Figure 2.12 Bridge system considered in Shao et al. (2014).

Cid et al. (2018) proposed a methodology for optimizing the cable system of multi-span cable-stayed bridges with crossing cables. In the process of optimization, the number of cables on the deck was considered as a discrete variable while the cable anchor positions, cross sectional areas and post-tensioning of cable forces were considered as continuous design variables. Queensferry Crossing Bridge was selected to demonstrate the methodology.

While most of the studies on cable-stayed bridges were focused on improving or developing a new system as described above, Jin et al. (2016) carried out a study on using a new material for cables. Instead of having cables made of steel, they proposed to use carbon-fiber-reinforced plastic (CFRP) to replace the steel. It was reported that CFRP cables reduced the axial forces in the main girders by about 65%. Accordingly, the main span length was increased significantly and reached the typical span length for suspension bridges.

CHAPTER 3

BRIDGE DESCRIPTION AND MODELLING

3.1 Bridge Description

A 1408m-long partially earth-anchored cable-stayed bridge with crossing stay cables proposed in Shao et al. (2014) was selected for this study. The selection was made for the following reasons: (1) partially earth-anchored system performs better than earth-anchored system and self-anchored system as discussed in Chapter 2, (2) crossing stay cables could significantly reduce the axial force in the main span, which, in turn, would make the span longer, (3) the main span of 1408 m is the longest span length cited in the literature available. It is necessary to mention that Shao et al. (2014) provides very limited information on the geometrical configuration of the bridge proposed. Therefore, Shao et al. (2018), Bittner et al. (2007) and Zhang (2009) were used as additional sources to get information missing in Shao et al. (2014) but required for the present study, in particular, the geometry of the pylons. Therefore, the bridge considered in the present study is not exactly the same as the one studied in Shao et al. (2014)[1].

Figure 3.1 shows the elevation view of the bridge considered in this study. It has 7 spans, 122m+120m+300m+1408m+300m+120m+122m. In the figure, label *L* and label *R* stand for the cables on the left and right side of Pylon 1, respectively. Given the symmetrical arrangement of the cables, the labels *L* and *R,* and cable numbering on Pylon 2 are reversed compared with Pylon 1.

[1] I tried my best to have geometry of the bridge match that used by Shao et al. (2014) as close as possible.

As seen in Fig. 3.1, there are 54 cables on each side of Pylon 1, in which 20 cables in the side span are anchored to a 58m-wide block on the ground. There are in total 432 cables installed from both sides of the deck (= 216 cable/per side x 2 sides) while 40 crossing stay cables are used in the main span on each side of the deck.

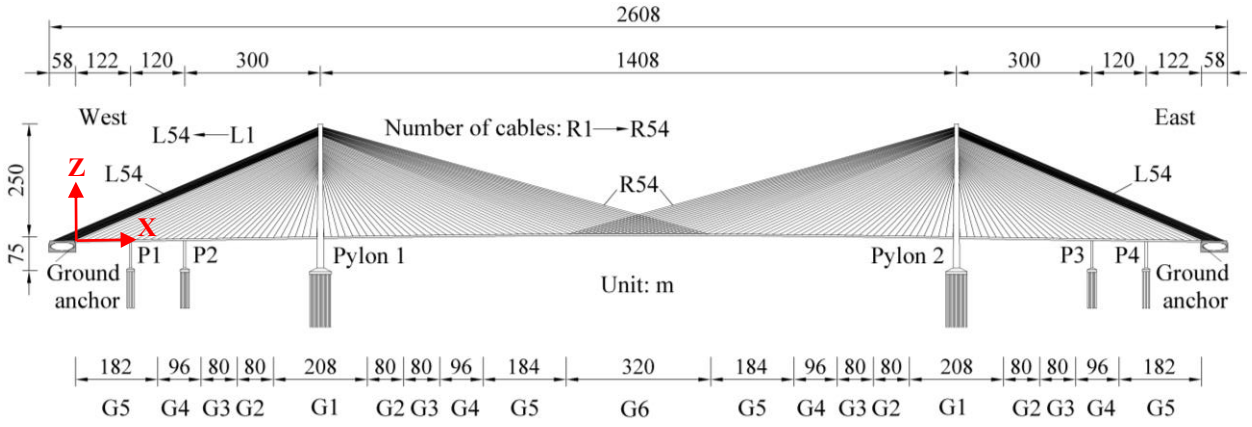

Figure 3.1 Elevation view of the bridge under examination as Shao et al. (2014).

Deck

Figure 3.2a presents the cross section of the main girder, which is orthotropic steel box girder, and Figure 3.2b is a photo of one girder segment before it is lifted into position during construction. The deck width is 42.4 m and the depth is 4.5 m measured at the centre of the section. The top plate thickness is between 6 – 18 mm while the bottom one is between 6 – 16 mm. As seen in Fig. 3.2, U-troughs are provided under the top steel plate to prevent the main girder from over stressing. Diaphragms were installed in both transverse and longitudinal directions. The girder is continuous cross all the seven spans.

(a)

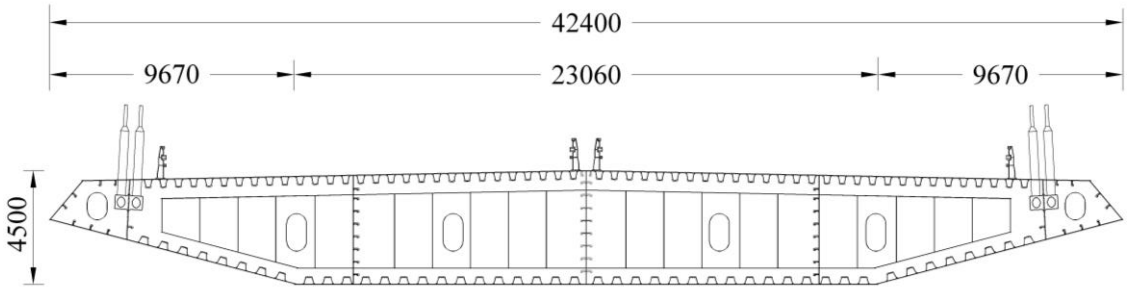

Unit: mm

(b)

Figure 3.2 Geometry of the girder: (a) cross section provided in Shao et al. (2018); (b) photo of the girder taken during construction (www.alamy.com, Image ID:P64RMN).

Pylon

Figure 3.3 shows the geometric configuration of the pylons considered in this study. Please take note the dimensions given in Fig. 3.3 were estimated based on the information on Sutong bridge given in Bittner et al. (2007) due to lack of information in Shao et al. (2014). As illustrated in Fig. 3.3, the total height of the pylon is 321.1 m, in which the heights of the upper, middle and lower legs are 111.8 m, 144.3 m, and 65 m, respectively.

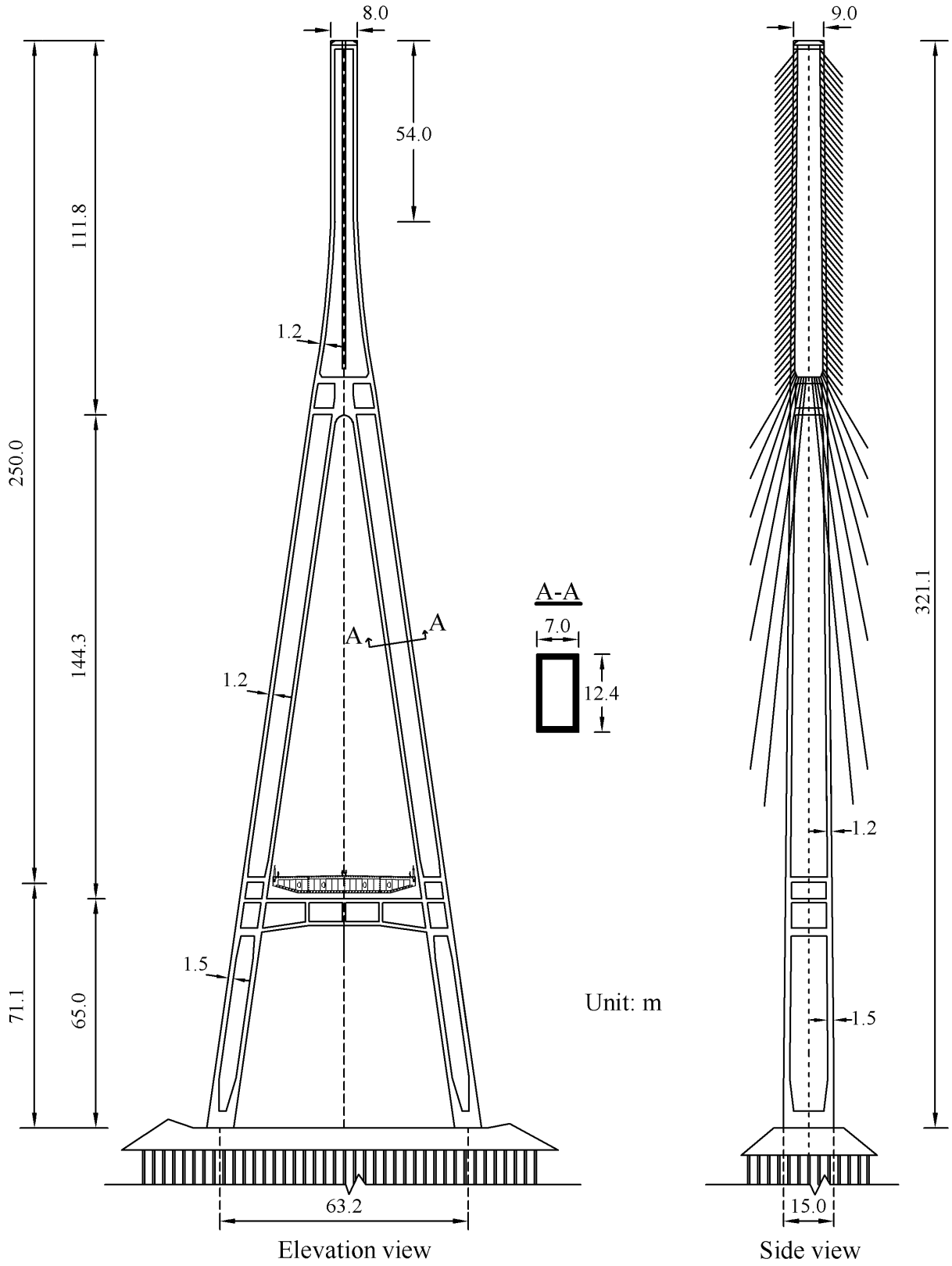

Figure 3.3 Pylon geometry.

Bearings

All the bearings on the bridge allow the movement of the girders in the longitudinal direction and they restrain the movement in the transverse direction; rotations in all the three directions (x, y, and z, see Fig. 3.1) are allowed.

3.2 Design of Cables

Due to lack of information on the cables in Shao et al. (2014) and elsewhere, a preliminary design was conducted in this study in order to determine the axial force in the cables and the cross-sectional area of the cables.

3.2.1 Determination of cable forces

There are five methods commonly used to determine the cable forces and the initial shape of the bridge, and they are explained as follows,

- Optimization method reported in Negrão et al. (1997) and Simões et al (2000): Pareto solution was found indirectly by minimizing an unconstrained scalar function. The optimization is conducted by reducing the stress and deflection, which are the two major parameters considered in the scalar function in addition to the cost. Once the design variables are quantified, the optimum cable post-tensioning force can be determined.
- Wang's method: Wang et al. (1997) investigated four different methods in order to determine the optimum post-tensioning cable forces that would minimize the deformations and stresses in cables under dead loads. In each method, a specific response parameter is considered. For example, one of the methods is to determine cable forces by minimizing the summation of squares of the vertical displacements along the bridge deck.

- Force equilibrium method introduced by Chen et al. (2000): cable forces are considered as an independent variable to obtain desirable bending moments in the girder.
- Unit load method developed by Janjic et al. (2003): the predetermined bending moment distribution due to dead loads at selected points along the main girder is considered as a control parameter to optimize the tensile force in cables.
- Zero-displacement method by Wang et al. (1993): cable forces are adjusted by trial and error to obtain a reasonable initial shape of the bridge under dead loads, in which a desirable convergence tolerance for a given response is reached and the deflection at selected control points is minimized. In addition, this method considers the nonlinearity of cables, such as, larger displacement, cable sag, and P-Δ effects in the calculation.

Among the five methods described above, zero-displacement method proposed by Wang et al. (1993) was chosen in this study to determine the cable forces of the bridge due to its simplicity and convenience of the finite element analysis. Figure 3.4 outlines the steps followed in this study to determine the cable forces, and Table 3.1 provides the convergence tolerance criteria for the girder and pylon to determine if the analysis needs to be repeated. As an example, Table 3.2 summarizes the results for the nodes at the middle of the main span and the node at the top of Pylon 1 corresponding to iterations 0 (i.e., the initial stage when cables have not been tensioned yet), 1, 5 and 7 (i.e., the last iteration where convergence tolerance is accepted) while Figure 3.5 shows the deformed shape of the bridge associated with each iteration. It is necessary to mention that the main span in Fig. 3.5 is measured from Pylon 1 to the end of the last crossing cable, which is 864 m = 104+80+80+96+184+320 m (see Fig. 3.1), the side span is measured from Pylon 1 to the end of the last girder section (G5), which is 542 m = 122+120+300 m (see Fig. 3.1). For the design purpose, the cables within the side span and the main span presented

in Fig. 3.5 are divided into 22 groups labelled as (C1-C4, C5….C22) from the west end. Each cable group has 5 cables except Groups C11 and C12 in which each has 4 cables.

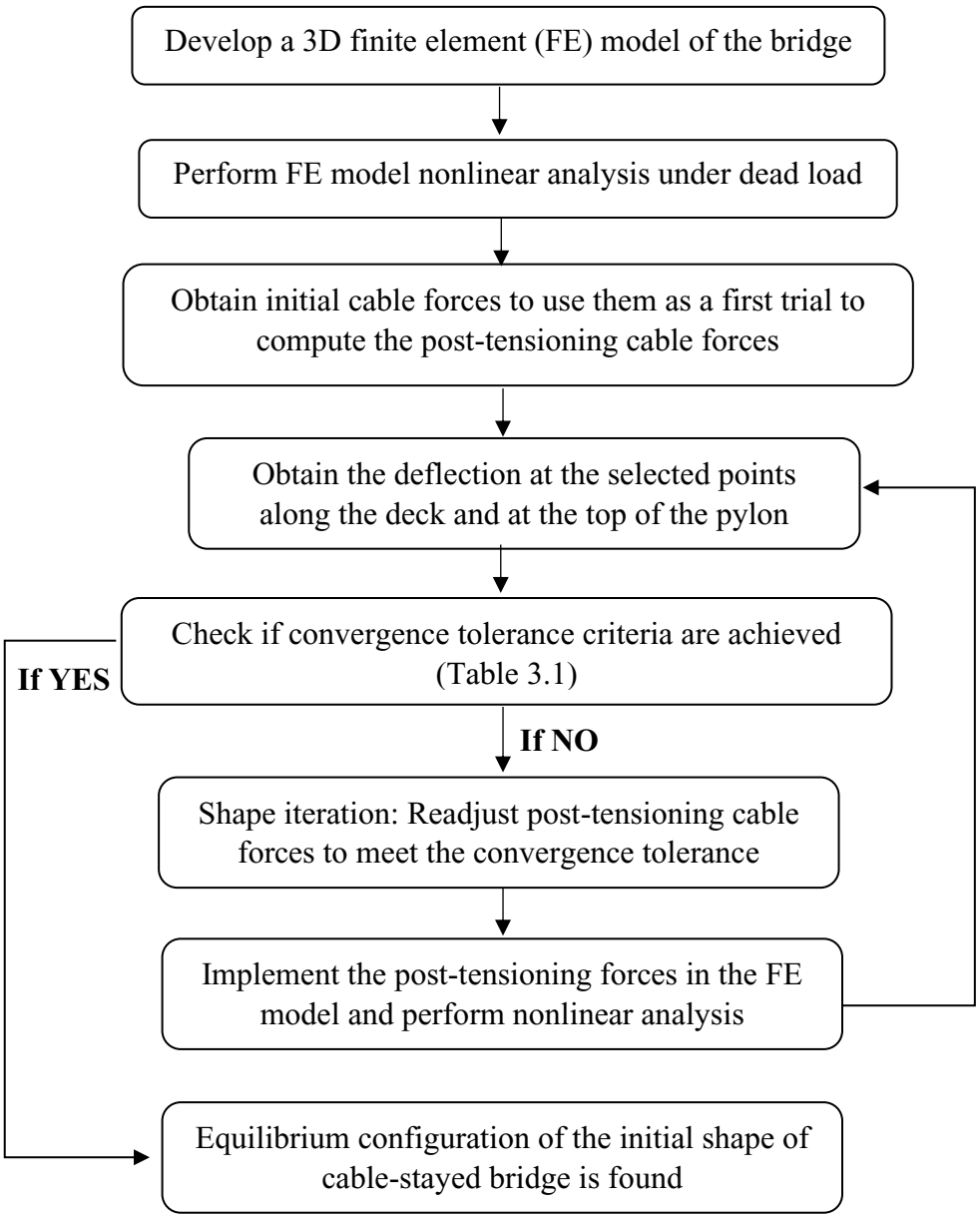

Figure 3.4 Flow chart for determination of cable forces in this study

Table 3.1 Convergence tolerance criteria proposed in Wang et al. (1993).

Component	Node location	Convergence tolerance limit
Girder	Middle of main span	$\frac{\lvert Vertical\ displacement\ at\ the\ node \rvert}{Span\ length} < 0.001$
	Middle between P2* and Pylon 1	
	Middle between P3 and Pylon 2	
	Middle between P1 and P2	
	Middle between P3 and P4	
	Middle between P1 and anchor block	
	Middle between P4 and anchor block	
Pylon	Top @ Pylon 1	$\frac{\lvert Horziontal\ displacement\ at\ the\ node \rvert}{Pylon\ height} < 0.001$
	Top @Pylon 2	

*Locations are illustrated in Fig. 3.1.

Table 3.2 Sample of iteration results.

Iteration number (i)	Cable group ID	Post-tensioning cable force (kN)	Middle of main span		Node at top of Pylon 1	
			Deflection (m)	Convergence	Deflection (m)	Convergence
i =0	C1-C4	0	-11.31	11.32/1408 = 8.03x0.001 **(Unaccepted)**	-1.94	1.8/325 = 5.54x0.001 **(Unaccepted)**
	C8					
	C11					
	C12					
	C16					
	C20					
i =1	C1-C4	3395	-5.8	5.8/1408 = 4.12x0.001 **(Unaccepted)**	-1.01	1.01/325= 3.11x0.001 **(Unaccepted)**
	C8	3530				
	C11	2500				
	C12	1025				
	C16	4045				
	C20	3454				
.....						
i =5	C1-C4	3498	-3.03	3.03/1408 = 2.15x0.001 **(Unaccepted)**	-0.54	0.54/325 = 1.66x0.001 **(Unaccepted)**
	C8	3675				
	C11	2200				
	C12	1413				
	C16	4073				
	C20	3502				
.....						
i =7	C1-C4	3620	0.04	0.04/1408 = 0.03x0.001 **(Accepted)**	0.1	0.1/325 = 0.31x0.001 **(Accepted)**
	C8	3850				
	C11	1900				
	C12	1800				
	C16	4130				
	C20	3550				

Iteration i=0
No post-tensioning force applied
Pylon lateral displacement: 1.94 m
Middle span displacement: 11.31m

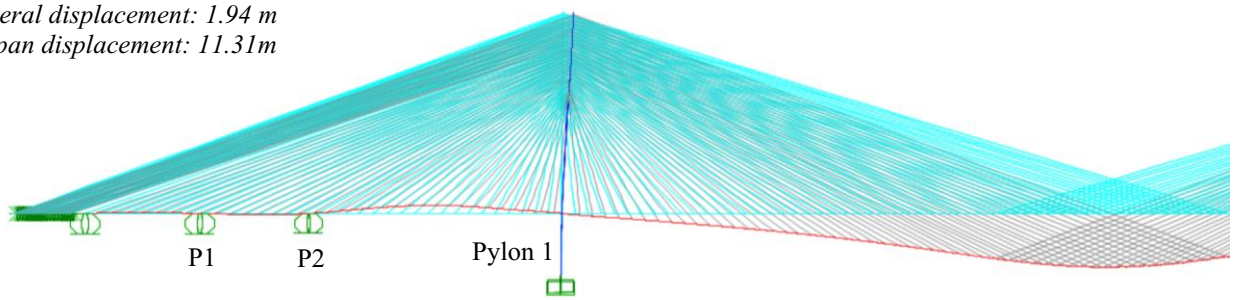

Iteration i=1
Post-tensioning force applied
Pylon lateral displacement: 1.01 m
Middle span displacement: 5.8 m

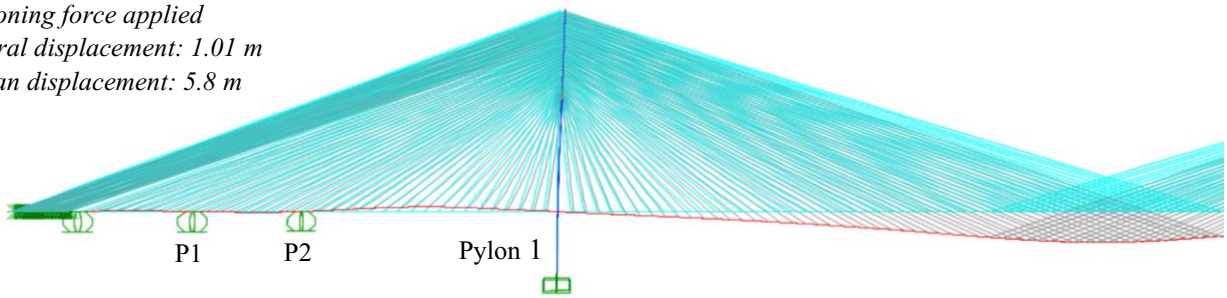

Iteration i=5
Post-tensioning force applied
Pylon lateral displacement: 0.54 m
Middle span displacement: 3.03 m

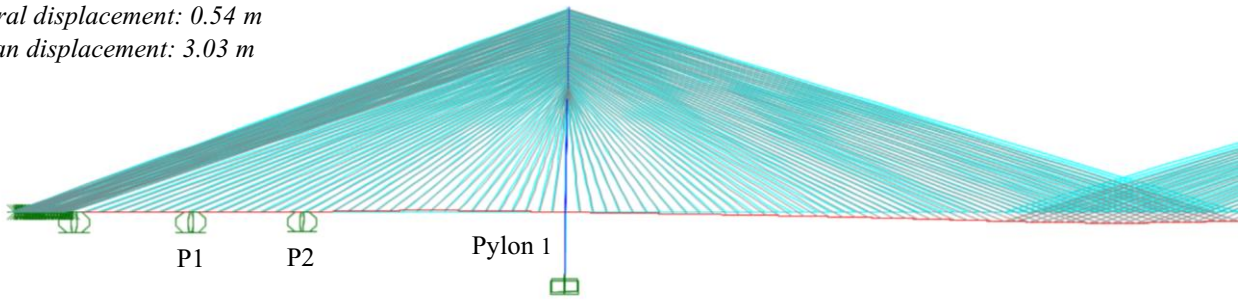

Iteration i=7
Post-tensioning force applied
Pylon lateral displacement: 0.10 m
Middle span displacement: 0.04 m

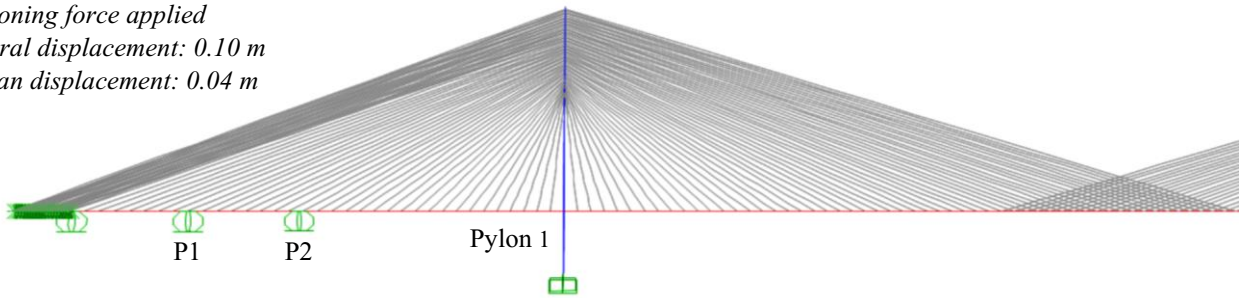

Figure 3.5 Bridge deformed shape at iterations 0, 1, 5, and 7.

3.2.2 Sizing of Cables

The sizing of the 22 groups of cables was conducted following the procedures given in Svensson (2012). In particular, the sectional area of cables was determined based on the allowable stress in the cables corresponding to 50% of the live load. As an example, a step-by-step calculation for sizing cable groups C1-C4 is presented below.

Step 1: Apply both lane load and dead load to the deck and run structural analysis using SAP2000. The lane load is 40 kN/m and it is distributed over the main span only. Besides the self-weight of the girder, the additional dead loads applied to the side and main spans are 134.5 kN/m and 87.5 kN/m, respectively, to include the wearing surface, utilities and ballast load over the side spans.

Step 2: Determine the maximum tensile force in cables of C1-C4 under live load and dead load (i.e., service limit state), T_{max}^{LL+DL}, which is 4230 kN given by SAP2000.

Step 3: Determine the maximum unbalanced force in the cable, ΔT due to live load only. It can be determined by summing up the force in the cable T1 when only the side span is loaded with the lane load and the force T2 in the same cable while only the main span is loaded. For C1-C4, T1 was found to be 0 kN and T2 was found to be 560 kN. Therefore, $\Delta T = 560$ kN.

Step 4: Determine the design tensile force T, which is the larger between T_{max}^{LL+DL} and ΔT. For C1 to C4, T = larger of (4230 kN, 560 kN) = 4230 kN.

Step 5: Determine the sectional area of cables by dividing the design force T by the design tensile strength of the strands, which is 744 MPa according to Shao et al. (2014). For C1-C4, the sectional area is found to be 0.00569 m^2 .

Step 6: Check the stress in the cable corresponding to 50% of the live load. For C1-C4, stress = 50% of ΔT/Area = 0.5*560/0.00569m^2 = 49.21MPa. In this study, the allowable stress was taken as 200 MPa as recommended in Svensson (2012). Since the stress in the cable is smaller than the allowable, the area determined is acceptable.

Figure 3.6 presents the forces in all 22 cable groups as well as the sectional area of cables in each group following the procedure described above. It is interesting to note in Fig. 3.6 that, for the main span, larger sectional area is found for cables in Groups 17 and 18, which is about 432 m from Pylon 1. In addition, the area of the crossing cables of Group 22 is about 57% of Group18.

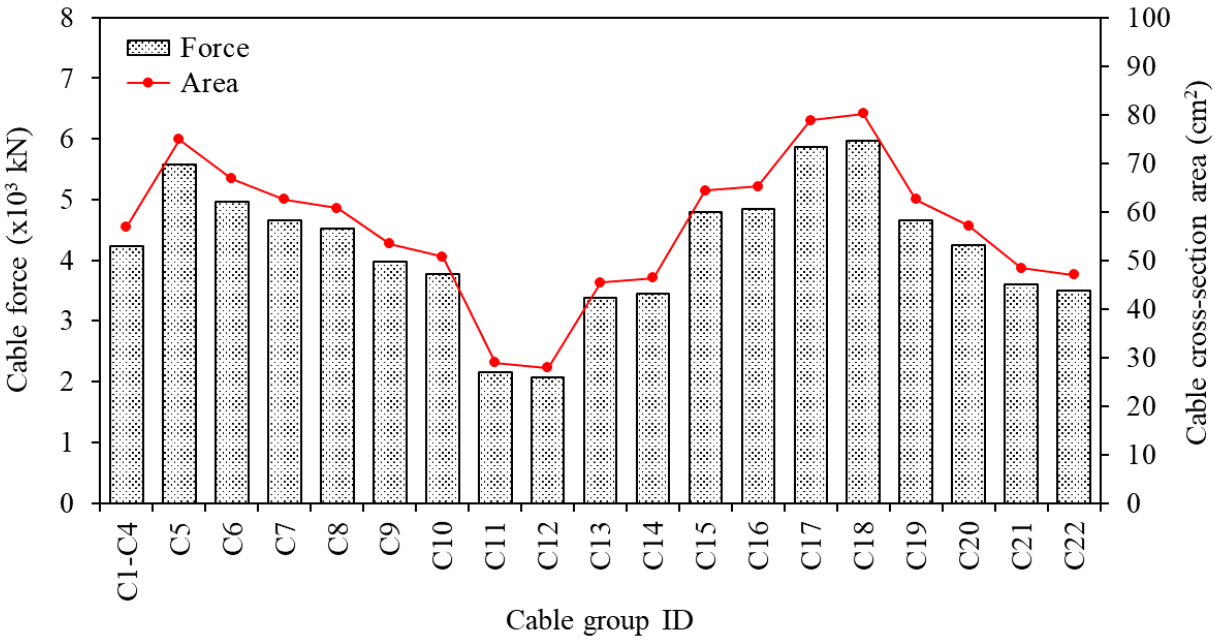

Figure 3.6 Results of cable force and cable cross-sectional area.

3.3 Bridge Modelling

The bridge considered in this study was modelled using SAP2000 (CSI, 2018). Figure 3.7 shows the 3D finite element model of the bridge developed for the analysis. Modelling of each component, such as superstructure, pylons, cables, etc. are described in detail in the section below.

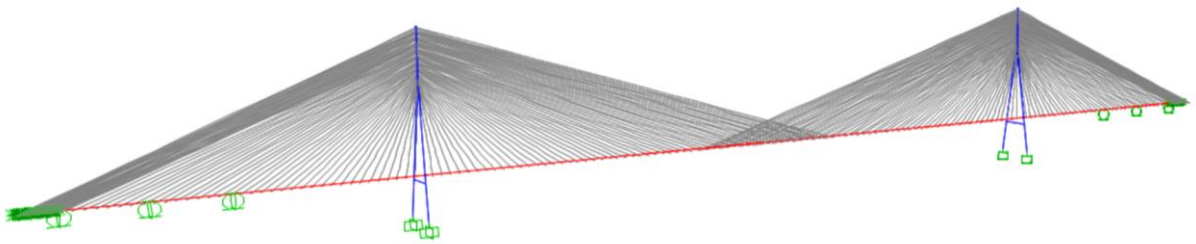

Figure 3.7 Three-dimensional finite element model of the bridge developed in SAP2000.

3.3.1 Elements

Superstructure

The superstructure is modelled as a "Spine" through the centroid of the girder section as illustrated in Fig. 3.7. The side span and the main span are modelled with 5 and 12 elements, respectively. Each element is defined as a frame element in SAP2000, and the cross-sectional dimensions of each element are assigned in SAP2000 in accordance with the girder group number G1-G6 depending on its location (Fig. 3.1). The anchorages of each pair of cables on both side of the deck are connected to the spine by a massless, horizontal rigid link, (Fig. 3.8)

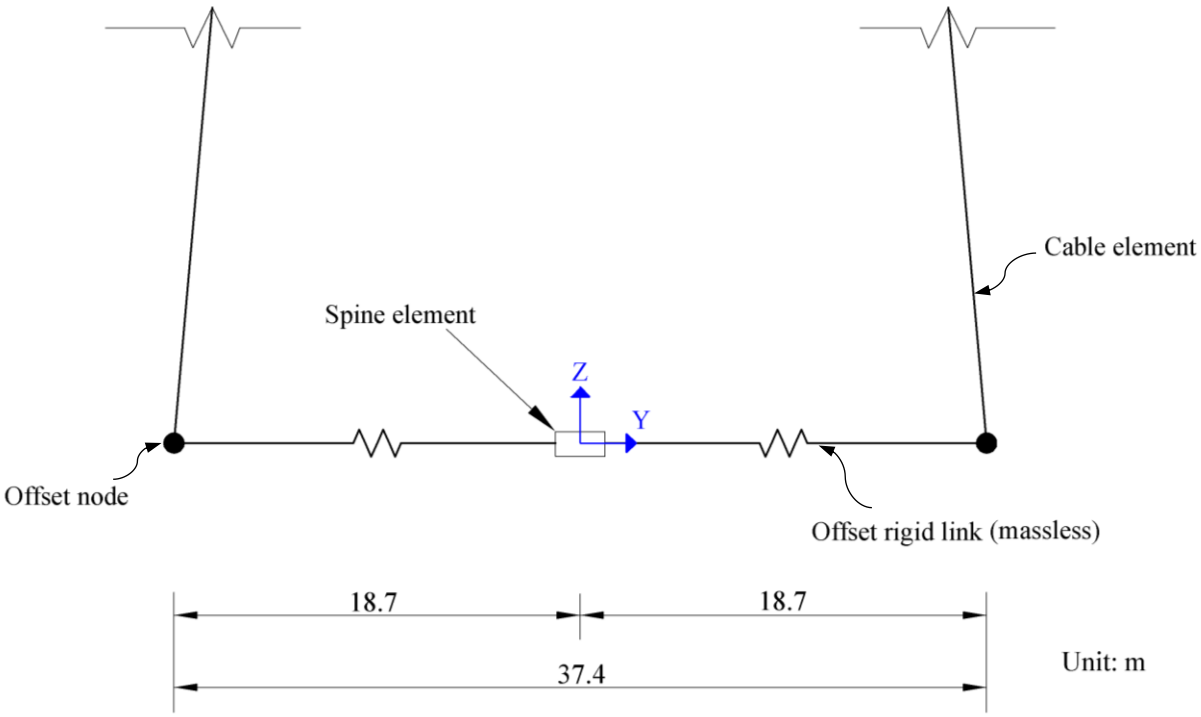

Figure 3.8 Finite element model of the superstructure.

Pylons

Based on the geometry, five nodes (black symbol in Fig. 3.9) were defined along each leg of the pylon, three nodes were defined on the upper part of the pylon. Every two adjacent nodes constitute one element, therefore, in total, twelve elements (= 5 elements/per leg + 2 elements on the top) were used to model the pylon. It is necessary to mention that four transvers elements (i.e., red lines in the figure) are added in the region where the two pylon legs merge together in order to simulate the interaction between the middle and upper legs.

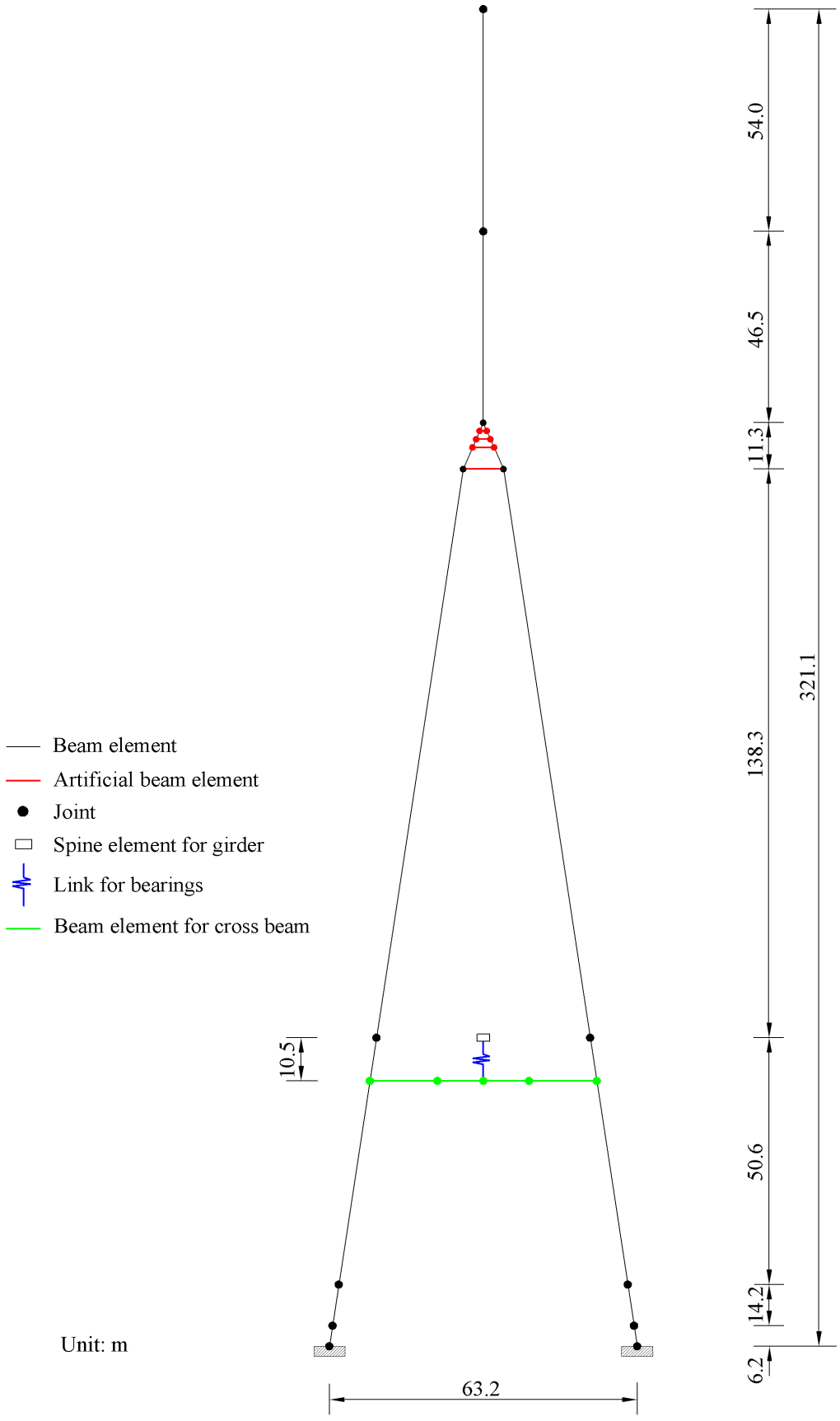

Figure 3.9 Finite element model of the pylon.

Cables

Cables are modelled using "single catenary non-linear cable element" defined in SAP2000. As described in Section 3.2.1, the cables are classified into 22 groups in which Group C11 and Group C12 each has 4 cables while each of the rest groups has 5 cables. Therefore, nineteen cable sections are defined in SAP2000. The end of each anchor cable is restrained from longitudinal, transverse, and vertical translation movements while rotations are allowed

Bearings

All the bearings at each pier or pylon are modelled using one linear link to connect the main girder to the cross beam underneath as shown in Fig. 3.9. At the pylon (i.e., Pylon 1 and Pylon 2, Fig. 3.1), the link restrains the transverse movement, vertical movement, and torsion. At the pier (i.e., P1, P2, P3, and P4, Fig. 3.1) only the translational degree of freedom in the vertical direction is restrained and the other five degrees (2 translation and 3 rotation) are free.

3.3.2 Boundary conditions

The bottom of each pylon is fully fixed, i.e., all the six degrees of freedom (translation and rotation in x, y, and z directions) are restrained. With respect to the boundary condition of the girder, both ends are restricted to move in the vertical direction. For the cables within the anchorage region, the end of each cable is restrained in all the degrees of freedom except the rotation about y- and z- axes (see the coordinate system in Fig. 3.1)

3.4 Model Validation

In order to validate the finite element model developed in the present study, both static and dynamic responses were compared with those provided in Shao et al. (2014). The static response is represented by the axial force in the girder while the dynamic response is represented by the mode shape and modal frequency.

3.4.1 Static response

Figure 3.10 presents the axial force distribution in the girder from the west end to the middle of the main span due to dead load obtained from the study and Shao et al. (2014). The origin of the horizontal axis is located at the starting point of the girder at the beginning of the side span at the west end (Fig. 3.1). It can be seen in the figure that a smaller difference of the results between this study and Shao et al. is observed in the main span and a relatively larger difference is found in the side span (Fig. 3.10). More specifically, the largest difference for the main span is about 13%, and for the side span is around 33%. It should be noted that the 13% difference for the main span was determined by considering the normal stay cables only, i.e., the crossing cables was eliminated in the calculation. This is because the axial force in the crossing cables were assumed to be zero in Shao et al. (2014). However, the maximum axial force in the cables obtained this study is very close to that reported in Shao et al. (2014), i.e., 199 MN vs. 194 MN.

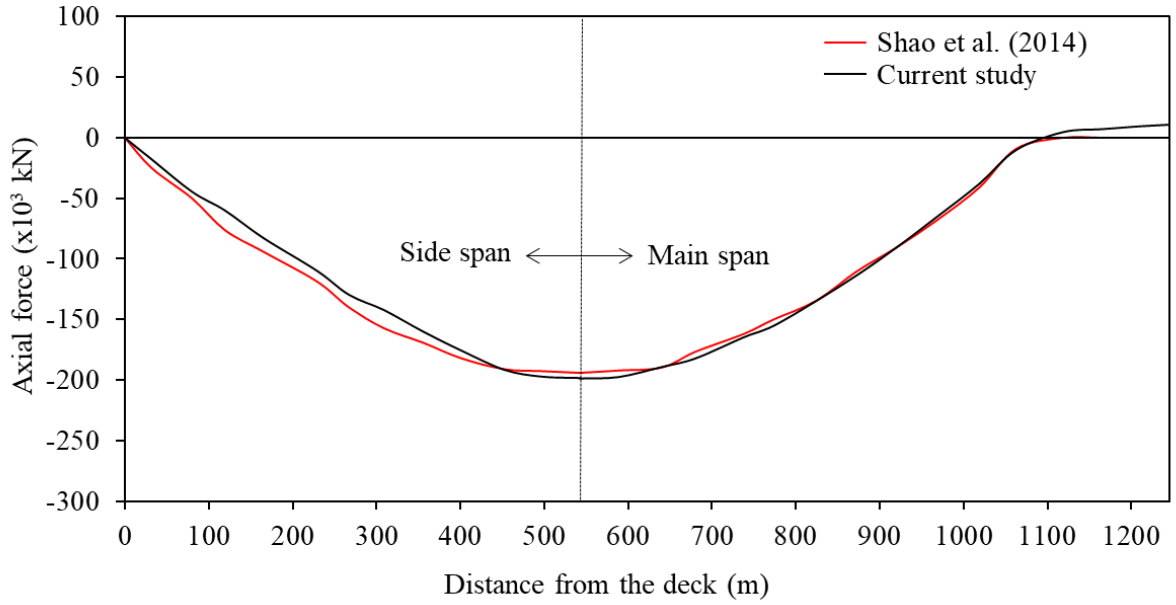

Figure 3.10 Axial force in the girder along the span.

3.4.2 Dynamic response

The comparison of the mode shape between this study and Shao et al. (2014) is shown in Fig. 3.11. The mode shapes selected are, (i) transverse symmetric bending of the girder, (ii) vertical symmetric bending of the girder, (iii) longitudinal floating of the girder, (iv) lateral bending of the pylons, and (v) symmetric torsion of the girder since they are available in Shao et al. (2014).

It can be seen in Fig. 3.11 that the same mode shapes as those reported in Shao et al. (2014) are obtained from this study except the mode number is shifted compared to Shao model. Furthermore, the frequency of the modes from the current study are compatible with those from Shao et al. (2014). Table 3.3 lists the frequencies of the first 10 modes as well as the direction of the vibration of each mode from the study. The results in Fig. 3.11 and Table 3.3 indicate that the motion of the bridge model is dominated by the girder. Specifically, the vibration is governed by the lateral bending of the bridge around z-axis (modes 1, 2, and 3) followed by the translation of the girder in the longitudinal direction (modes 5 and 7) and the oscillation of the girder in the main span in vertical direction. In total, 55 modes were

considered in the modal analysis to achieve a mass participation ratio greater than 90%. It is necessary to mention that a stiffness weighted damping (i.e., composite modal damping) of 5% was assigned to all the modes in the dynamic analysis.

Current study	**Shao et al. (2014)**
Mode 1: transverse symmetric bending of the girder  f = 0.042 Hz	Mode 1: transverse symmetric bending of the girder  f = 0.053 Hz
Mode 4: vertical symmetric bending of the girder  f = 0.143 Hz	Mode 3: vertical symmetric bending of the girder  f = 0.142 Hz
Mode 5: longitudinal floating of the girder  f = 0.153 Hz	Mode 6: longitudinal floating of the girder  f = 0.160 Hz
Mode 14: lateral bending of the pylons 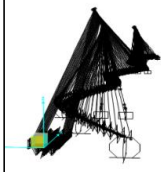 f = 0.394 Hz	Mode 14: lateral bending of the pylons  f = 0.374 Hz
Mode 31: symmetric torsion of the girder 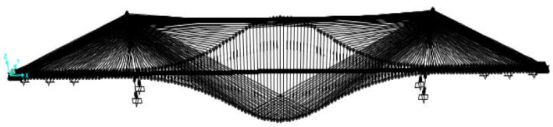 f = 0.790 Hz	Mode 30: symmetric torsion of the girder  f = 0.707 Hz

Figure 3.11 Mode shape comparison between current study and Shao et al. (2014).

Table 3.3 Dynamic characteristics of the bridge model.

Mode No.	Characteristics of vibration	Frequency (Hz)
1	First lateral symmetric bending of the girder	0.042
2	First lateral asymmetric bending of the girder	0.059
3	Second lateral symmetric bending of the girder	0.089
4	Vertical symmetric bending of the girder	0.143
5	First longitudinal floating of the girder	0.153
6	Second lateral asymmetric bending of the girder	0.187
7	Second longitudinal floating of the girder	0.205
8	Symmetric vertical oscillation of the main span girder	0.240
9	Asymmetric vertical oscillation of the main span girder	0.285
10	Third lateral symmetric bending of the girder	0.329

CHAPTER 4

ANALYSIS RESULTS

4.1 Overview

Since the objective of this study is to investigate the performance of a cable-stayed bridge due to different side-to-main span ratio, 5 additional ratios were tested in this study and they were 0.24, 0.27, 0.30, 0.33 and 0.36. It should be noted that the side to main span ratio of the original bridge was about 0.39 (= 122+120+300 m/1408 m, Fig. 3.1). For ease of understanding, Table 4.1 lists the 6 side-to-main ratios examined in the study along with the side span length for each case, which is measured from Pylon 1 on the west end and Pylon 2 on the east end.

Table 4.1 Side span lengths examined in the study.

Ratio / Item	0.24	0.27	0.30	0.33	0.36	0.39
Side span length (m)	338	380	422	465	507	524

During the examination, the following quantities of the parameters defined in the bridge considered in Shao et al. (2014) remain unchanged, (i) pylon height: 321.1 m, (ii) main span length: 1408 m, (iii) length of the region with crossing stay cables at the main span: 320m, (iv) total number of cables at the main span, (v) total number of cables at the side span, and (vi) location of piers (P1 to P4) relative to the side span length: in particular P1 and P2 are located at about 55% and 78% of the span length away from Pylon 1; P3 and P4 are placed in the same manner, but measured from Pylon 2.

The response parameters selected for the investigation are as follows,

- Girder: axial force, bending moment, stress at the extreme top and bottom fibers, vertical deflection, and longitudinal movement
- Cable: axial force
- Pylon: bending moment at the bottom of the pylon, and lateral displacement
- Pier: uplifting force
- Anchorage: horizontal and vertical forces

The three loads considered for the investigation are dead load, traffic load and earthquake load in which the first loads are used to represent the bridge static response while the last to represent the bridge dynamic response. With respect to the traffic load, only the uniform part of the load defined in CHBDC lane load was considered, i.e., truck load was not applied to deck. This is because, for the super long span bridges, uniform load will govern the response not the truck load as reported in Hassan et al. (2013). In the analysis, the distribution of the lane load was considered in three cases described below and the largest absolute amount of the three cases is taken as the response from the traffic load.

- Case I: Two side spans are loaded, i.e., main span is not loaded
- Case II: Main span is loaded, i.e., two side spans are not loaded
- Cases III: Entire bridge (two side spans and the main span) is loaded

4.2 Bridge Response under Static Loading

4.2.1 Girder

Axial force

Figure 4.1 presents the girder axial force distribution for half of the bridge length due to dead load for the six cases of the side-to-main span ratio examined. In Fig. 4.1, the negative and positive values on the vertical axis represent the compression and tension force, respectively. The origion axis of the horziontal axis in Fig. 4.1 and all other similar figures hereafter is consistent with the origin of x-axis as illustrated in Fig. 3.1. Due to the symmetry of the bridge, the axial forces and bending moments in the girder presented in the figures in this chapter are plotted up to the center of the main span.

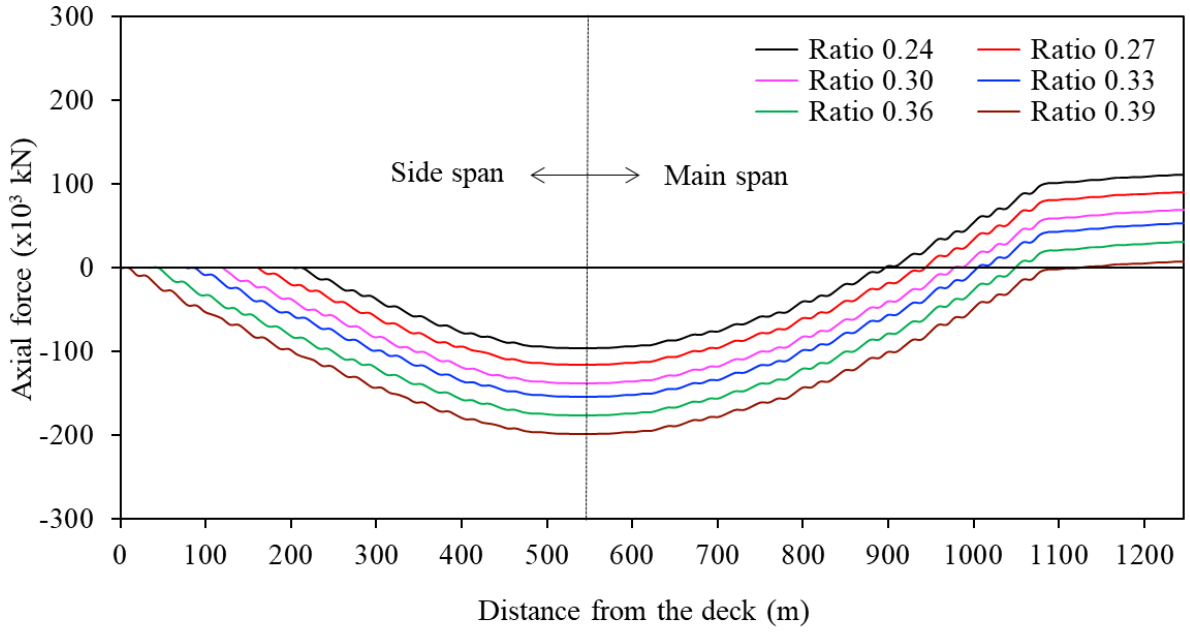

Figure 4.1 Girder axial force diagram for dead load.

It can be seen in the figure that, with the increasing of the side-to-main span ratio, a great amount of the compressive force is developed at the entire side span and part of the main span. In terms of the tensile force, a relatively large amount is solely concentrated in the region

with crossing cables. Furthermore, it is found that larger side-to-main span ratio leads to smaller tensile force. For example, for the ratio of 0.24, the maximum tension is about $111x10^3$ kN while for the ratio of 0.39, the maximum is about $7.7x10^3$ kN (Table 4.2). Such difference indicates that crossing cables are very efficient for larger side-to-main span ratio.

Table 4.2 Maximum axial force in girder.

Side-to-main span ratio	Side span @ 542m ($x10^3$ kN)				Main span @ 1246m ($x10^3$ kN)				Ratio of compression to tension
	DL	DL+ LL	LL*	$\frac{LL}{DL+LL}$	DL	DL+ LL	LL	$\frac{LL}{DL+LL}$	
0.24	-96	-110	-14	0.13	111	135	24	0.18	0.82
0.27	-116	-132	-17	0.13	90	111	21	0.19	1.18
0.30	-138	-158	-20	0.13	69	88	18	0.21	1.80
0.33	-154	-176	-22	0.13	54	70	16	0.23	2.53
0.36	-177	-202	-25	0.12	31	44	13	0.30	4.61
0.39	-199	-227	-28	0.12	8	18	10	0.57	12.55

*LL is referred as traffic load.

Figure 4.2 shows the girder axial force due to a combination of dead load and traffic load. By comparing the results in Fig.4.1 with Fig. 4.2, it was found that traffic load makes less contribution to the compressive force but larger contribution to the tensile force. Furthermore, it is interesting to note that, for the compressive force in the girder, the percentage of the response induced by the traffic load is about 12-13% of the total given by the combination of dead load and traffic load for all the 6 ratios in question (Table 4.1). This finding is expected given the fact that dead load normally governs the deck reponse not traffic load for long span bridges. However, for the tensile force, with the increase of the side-to-main span ratio, traffic load becomes dominant as illustrated in Table 4.2. For example, for the side-to-main span ratio

of 0.24, the axial force generated by traffic load is about 18% of that by dead load. However, when the side-to-span ratio raises up to 0.36, the percentage is increased to 30%. When the side-to-span ratio reaches 0.39, the compressive force in the side span is increased significantly, meanwhile, the tensile force at the main span developed by traffic load becomes 1.25 times dead load, which is extremly greater than the observation from the other cases. Table 4.2 also provides the ratios of the maximum compressive force to the maxium tensile force along the length of the bridge, which range from 0.82 for the ratio of 0.24 to 12.55 for the ratio of 0.39.

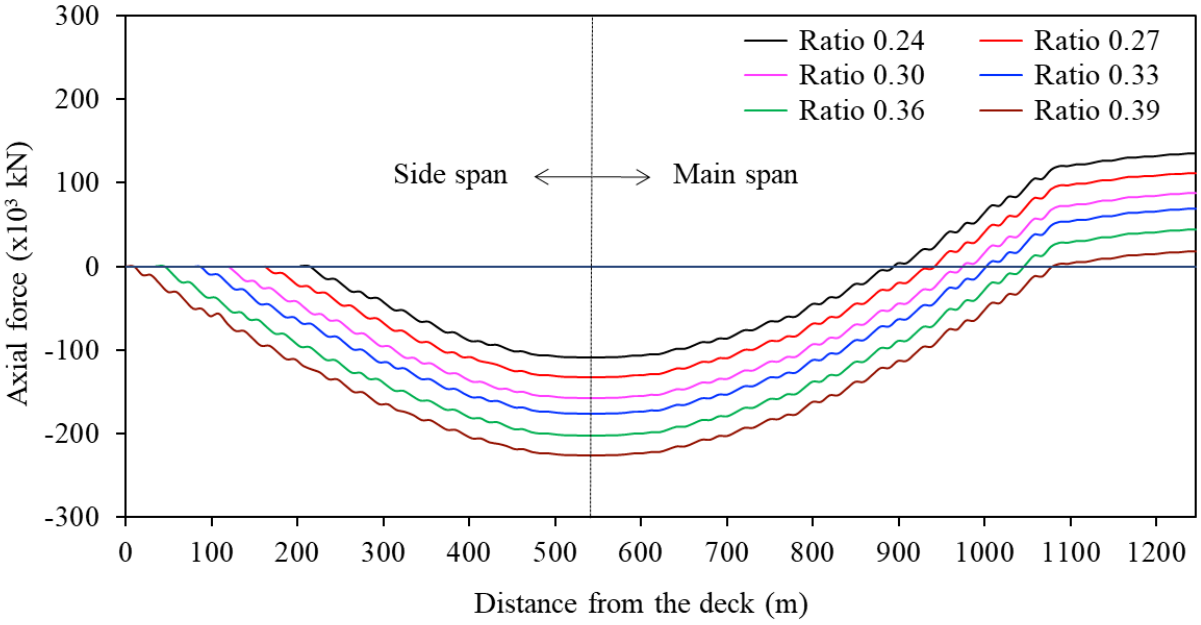

Figure 4.2 Girder axial force distribution along the span for combined dead load and traffic load.

Bending moment

Figure 4.3 shows the bending moment diagram for the girder due to dead load. Only the results for the side-to-main span ratio of 0.24 (lowest), 0.33 and 0.39 (largest) are illustrated in the figure. This is because the diagrams for other ratios are similar to those presented in Fig. 4.3 except the quantities are slightly different.

The results of the bending moment in the girder due to dead load in Fig. 4.3 show that larger side-to-main span ratio creates larger bending moment at the side span and vice versa. For example, the maximum negative bending moment corresponding to the ratio of 0.39 is about 5 times that corresponding to the ratio of 0.24. However, the difference of the bending moment at the main span from different ratios is relatively small. This is because the self-weight of the girder is directly proportional to the side span length, which has a direct effect on the bending moment.

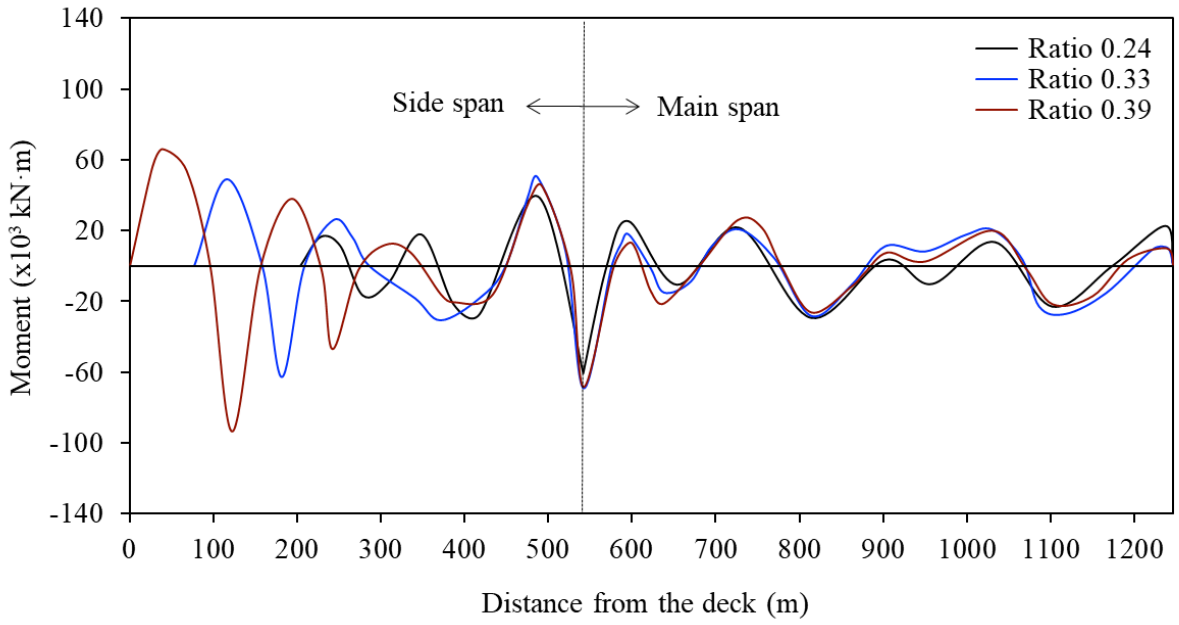

Figure 4.3 Girder bending moment distribution along the span for dead load

The observation of the results from the bending moment envelopes shown in Fig. 4.4 is consistent with that in Fig. 4.3. It can also be seen in Fig. 4.4 that the changing of the side-to-main span ratio has no significant effect on the main span. Furthermore, the bending moments in the side span are much larger than those in the main span. One of the reasons is because of the additional uniform load of 47kN/m (ballast load) applied on the side span.

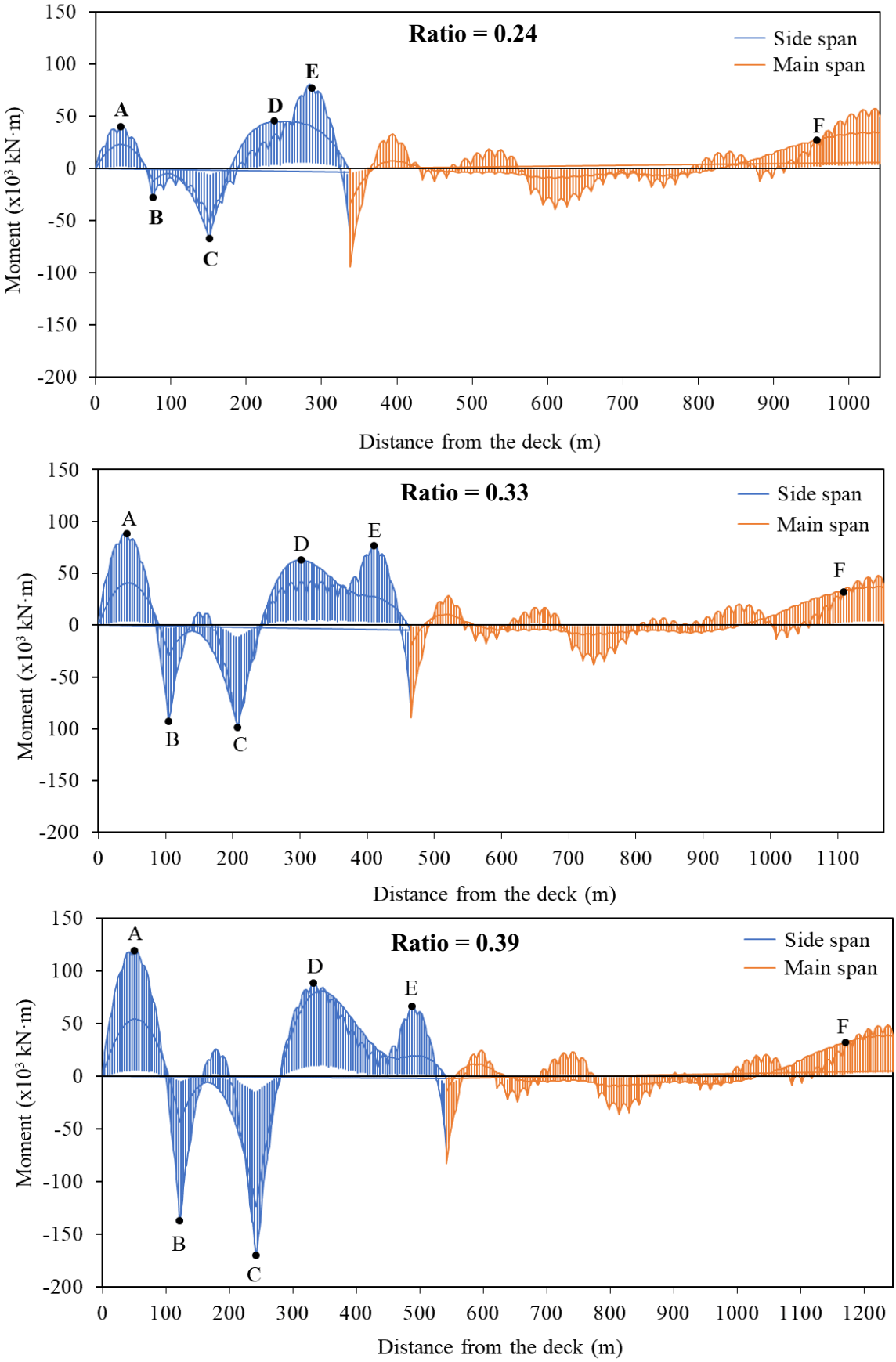

Figure 4.4 Girder moment envelope for combined dead load and traffic load.

As expected, the maximum negative moment occurs at the location of the two auxiliary piers P1 and P2. However, the location where the maximum positive moment occurs depends on the ratio of the side-to-main span ratio. For example, for the ratio of 0.24, the maximum moment is located at point E while the maximum moment is located at point A for the ratio of 0.39.

In order to compare the maximum bending moment among the 6 cases, Table 4.3 summarizes the moments at the 6 typical points selected (i.e., from Point A to Point F shown in Fig. 4.4). The major findings from the results in Table 4.3 are as follows,

- The moment increases with the increasing of the side-to-main span ratio.
- For side-to-main span ratios of 0.36 and 0.39, the bending moments are very close except for Point B, where the difference between the two cases is about 20%.
- The bending moment for Point F is almost the same for all the cases. Compared with the other 5 points (A to E), the moment at Point F is quite small. This is another benefit of using crossing cables besides reducing the tensile force in the girder.
- With respect to the bending moment for Points A to E, there is a big difference on the results. Specifically, the ratio of the largest to the least in each case ranges from 4.89 (for Point B) to 1.14 (for Point E).

Table 4.3 Girder bending moment (kN·m) at selected points for combined dead load and traffic load.

Point	Location	Side-to-main span ratio						Ratio of max. to min.
		0.24	0.27	0.30	0.33	0.36	0.39	
A	Middle between P1 and ground anchor	40	57	76	88	113	120	3.00
B	P1	-28	-49	-72	-93	-119	-137	4.89
C	P2	-67	-77	-88	-99	-158	-170	2.54
D	90 ~100 m from P2	46	50	56	63	91	88	1.91
E	40~ 50 m from Pylon 1	77	78	79	77	60	67	1.32
F	Inside the zone with crossing cables	28	29	29	30	31	32	1.14

Stress

Tables 4.4 and 4.5 provide the maximum tensile stress and maximum compressive stress in the girder due to a combination of dead load and traffic load, respectively. The stresses are presented for both the extreme bottom and top fibres. It can be seen in Table 4.4 that the tensile stress in the girder is governed by the main span except in the following two cases, (i) ratio of 0.39 for both top and bottom fibre, and (ii) ratio of 0.36 for the top fibre, where the side span governs. In addition, it should be noted there is a significant difference on the stress between main span and side span for a relatively small side-to-main span ratio. For example, for the span ratio of 0.24, for the bottom fibre, the stress at the main span is about 7 times that at the side span. Such a result indicates ratio of 0.24 is not economical and efficient. With respect to the compressive stress (Table 4.5), it is interesing to note that the stress on the bottom fiber is the same for both side and main spans for all the ratios examined. Regarding the top fibre,

although the stress is not exactly the same for the side span and main span, it is very close. Furthermore, the stresses obtained from all the cases do not exceed the steel yielding strength of 275 MPa considred in the design.

Table 4.4 Maximum tensile stress (MPa) in girder due to combined dead load and traffic load.

Side-to-main span ratio	Extreme bottom fibre		Extreme top fibre	
	Side span	Main span	Side span	Main span
0.24	13.9	100.7	24.2	75.3
0.27	15.9	81.8	27.9	63.3
0.30	18.8	69.7	31.8	49.2
0.33	26.5	58.3	35.9	38.0
0.36	33.4	45.6	40.6	22.9
0.39	36.3	31.7	44.7	7.7
Average	**24.1**	**64.6**	**34.2**	**42.7**

Table 4.5 Maximum compressive stress (MPa) in girder due to combined dead load and traffic load.

Side-to-main span ratio	Extreme bottom fibre		Extreme top fibre	
	Side span	Main span	Side span	Main span
0.24	-78.2	-78.2	-61.3	-56.9
0.27	-90.0	-90.0	-72.1	-65.8
0.30	-101.4	-101.4	-84.8	-76.6
0.33	-107.6	-107.6	-93.1	-85.3
0.36	-113.3	-113.3	-101.1	-98.9
0.39	-127.4	-127.4	-113.9	-107.5
Average	**-103.0**	**-103.0**	**-87.7**	**-81.8**

Displacement

Deck vertical deflection is a major concern in the bridge design as it will affect the comfort of bridge users. Given this, the maximum vertical deflection of the deck under traffic load was checked and the results are summarized in Table 4.6. As expected, the deflection of the main span is much larger than that of the side span. Furthermore, the maximum deflection at the main span for different side-to-main span ratio does not vary too much. More specifically, the difference between the deflection from the ratios of 0.24 and 0.39 is only about 10%. In addition, the maximum deflection in all the cases does not exceed the allowable deflection limit of L/400 for cable stayed bridges, which is 3.52m in this case for L of 1408 m. It is important to mention that the girder vertical displacement due to dead load is supposed to be zero according to the Zero Displacement method adopted to design cables in this study. In case the displacement is not zero, it should satisfy the tolerance limit given in Table 3.1, Chapter 3.

Table 4.6 Vertical deck deflection (cm) under traffic load.

Location	Side-to-main span ratio					
	0.24	0.27	0.30	0.33	0.36	0.39
Middle of the main span	193	191	196	198	204	210
Middle between P2 and Pylon 1	12	14	18	23	30	36

The longitudinal movements of the girder at the location of the pylon is -3 cm for ratio of 0.24, -1 cm for ratio of 0.27, 5 cm for ratio of 0.30, 9 cm for ratio of 0.33, 13 cm for ratio of 0.36, and 17 cm for ratio of 0.39. The negative displacement indicates the girder moves towards the west (see Fig. 3.1). As the side-to-main span ratio decreases, the longitudinal movement of the girder decreases and tends to move toward the abutment at the end of the side span. The maximum movement observed is 17 cm corresponding to the side-to-main span ratio of 0.39,

while the minimum movement is 1 cm corresponding to the ratio of 0.27. They both could be easily accommodated by expansion joints.

4.2.2 Cable force

Table 4.7 provides the maximum force for each cable group at the side span under a combination of dead load and traffic load, which was used to sizing cables as described in Chapter 3. The shaded values in the table are referred to cables anchored on the ground. For ease of undertsanding, a ratio of maximum cable force to the minimum for each cable group from the 6 different side-to-main span ratios is also presented in the table. It can be seen in the table that the difference in all cases is not greater than 10% except for Group 9, in which the difference reaches 19%. The results in Table 4.7 also show that, for Group 11, which is very close to Pylon 1, the maximum cable force from all the side-to-main span ratios examined is the same. The same observation was also found in other cable groups at the main span, i.e., Groups 12-22. Such a result indicates that the side-to-main span ratio does not affect the forces in cables.

Table 4.7 Cable force (kN) due to the dead load and traffic load.

Cable group ID	Side-to-main span ratio						Ratio of max. to min.
	0.24	0.27	0.30	0.33	0.36	0.39	
C1-C4	4555	4460	4400	4360	4390	4230	1.08
C5	5680	5640	5590	5320	5300	5570	1.07
C6	4940	4920	4870	5020	4955	4970	1.03
C7	4510	4510	4530	4530	4550	4650	1.03
C8	4580	4610	4660	4690	4530	4520	1.04
C9	4450	4340	4185	4080	3750	3975	1.19
C10	3620	3560	3600	3700	3900	3775	1.10
C11	2151	2151	2151	2155	2150	2151	1.00

4.2.3 Pylon

Table 4.8 shows the maximum bending moment in the pylon and the maximum lateral deflection at the top of the pylon. Both are due to the combination of dead load and traffic load. Please take note that the bending moment is recorded at the bottom of the pylon. The results in the table shows that both bending moment and deflection increase almost linearly with the increasing of the side-to-main span ratio. This is because the pylon behaves elastically under the two loads. The results for the pylon lateral deflection are expected, i.e., a larger deflection is obtained from a larger side-to-main span ratio. The maximum pylon deflection ratio observed from the cases is 0.14% (= 0.45/321*100), which is relatively small for a massive pylon like the one considered in the study.

Table 4.8 Pylon bending moment and lateral displacement.

Side-to-main span ratio	Moment (x10^3 kN·m)	Deflection (cm)
0.24	525.8	27
0.27	546.6	32
0.30	622.2	35
0.33	695.8	39
0.36	758.2	36
0.39	777.8	45

4.2.4 Pier

It is a general practice to limit side-to-main span ratio in choosing a side span length for continuous bridges. This is mainly to avoid excessive uplift force to be induced at the side span. For this purpose, uplift forces corresponding to the six side-to-main span ratios were evaluated in this study, and the results are summarized in Table 4.9. Given the symmetry of the bridge, only the forces in P1 (i.e., Pier 1) and P2 (i.e., Pier 2) on the west end of the bridge are provided. It is necessary to mention that the forces given in Table 4.9 are due to traffic load. The results

clearly show that traffic load generates larger uplift force in P2, which is closer to Pylon 1, it develops smaller force in P1, which is far from Pylon 1. As shown in Table 4.9, the uplift force in P2 can be approximately 1.5 to 2 times larger than in P1.

Table 4.9 Traffic load induced uplift force (kN) in piers.

Location	Side-to-main span ratio					
	0.24	0.27	0.30	0.33	0.36	0.39
P1	2944	3177	3374	3686	4004	4338
P2	5700	5915	6056	6306	6326	6524
Ratio of force in P2 to P1	**1.94**	**1.86**	**1.79**	**1.71**	**1.58**	**1.50**

4.2.5 Anchorage force

One of the principles for the partially earth-anchored system is to use back-stay cables to transmit the axial force in cables to the anchors located at the end of the side span. Accordingly, the forces in the cables in the earth anchored zone will significantly affect the design of anchors. Figure 4.5 illustrates the horizonal and vertical anchorage forces from the combination of dead load and traffic load. As expected, the horizontal force is much larger (at least two times) than the vertical one. Furthermore, it can be seen clearly in the figure that both forces decrease with the increase of the side-to-main span ratio. The ratios of the maximum to the minimum force for horizonal force and vertical force among the six side-to-main span ratios examined are about 1.8 and 2.5, respectively.

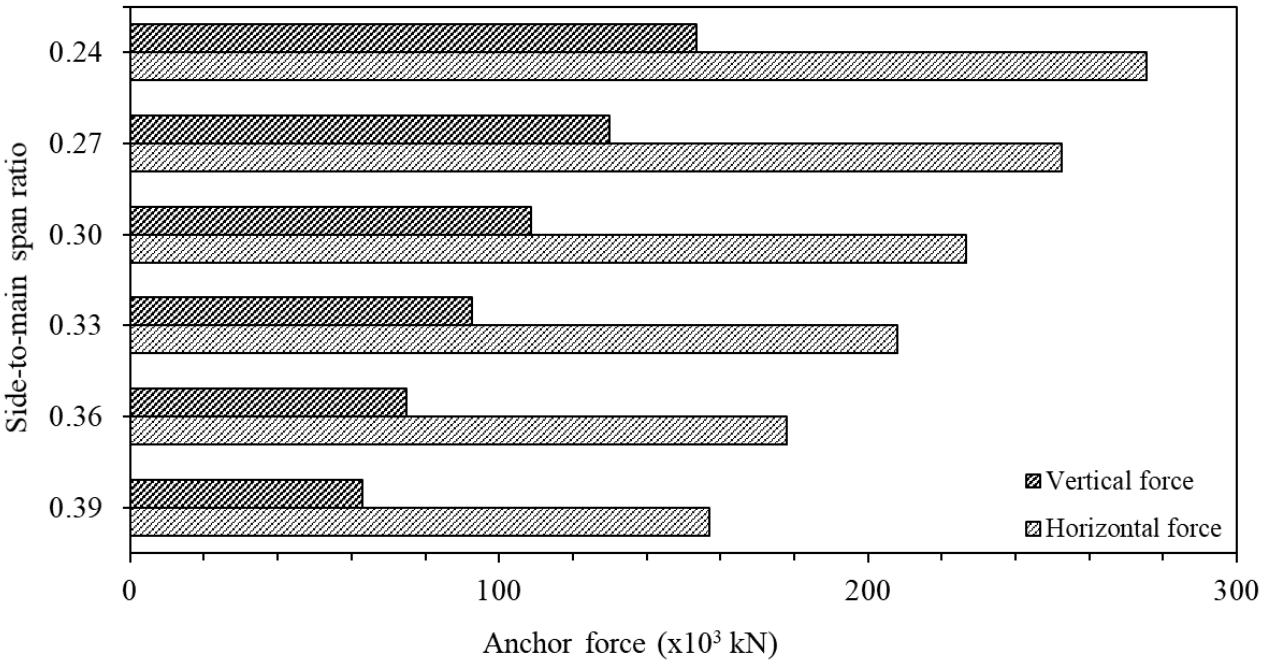

Figure 4.5 Vertical and horizontal components of anchorage force due to combined dead load and traffic load.

4.3 Bridge Response under Dynamic Loading

In addition to investigate the static response of the cable-stayed bridge for different side-to-main span ratio, dynamic response of the bridge was evaluated. In this study, earthquake load was selected to represent the dynamic load. EI Centro earthquake record was used as ground motion excitation and applied in the bridge longitudinal direction. Figure 4.6 shows the acceleration and displacement time histories of the record. The response parameters considered in the seismic analysis are the same as those in the static analysis.

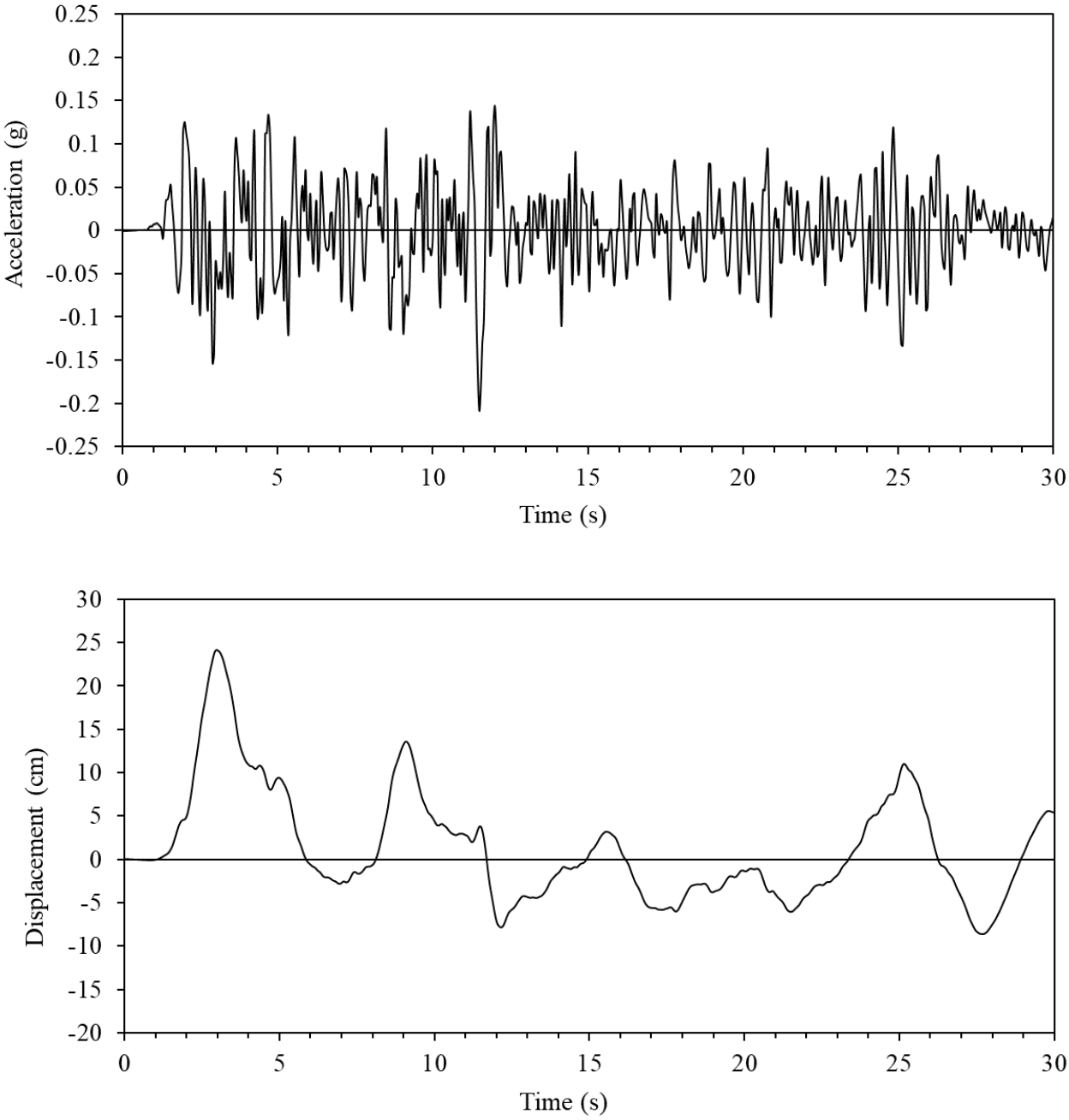

Figure 4.6 Acceleration and displacement time history of the EI Centro earthquake record

4.3.1 Girder

Axial force

Figure 4.7 presents the maximum tensile and compressive forces developed in the girder due to earthquake load (EQ). The results in the figure show that tensile force is slightly larger than compressive force. The largest response occurs in the vicinity of the Pylon. In the region around the middle of the main span, the seismic repsonse is almost the same for all the side-to-main span ratios under examination, as shown in Fig. 4.7. In addition, it is observed in Fig. 4.7 that very little tension force is developed in the shaded zone with crossing cables. This indicates the efficiency of crossing cables in this bridge system in question. Furthermore, by comparing the resutls in Table 4.2 with the results in Fig. 4.7, it can be concluded that the axial force from EQ is much smaller than that from traffic load.

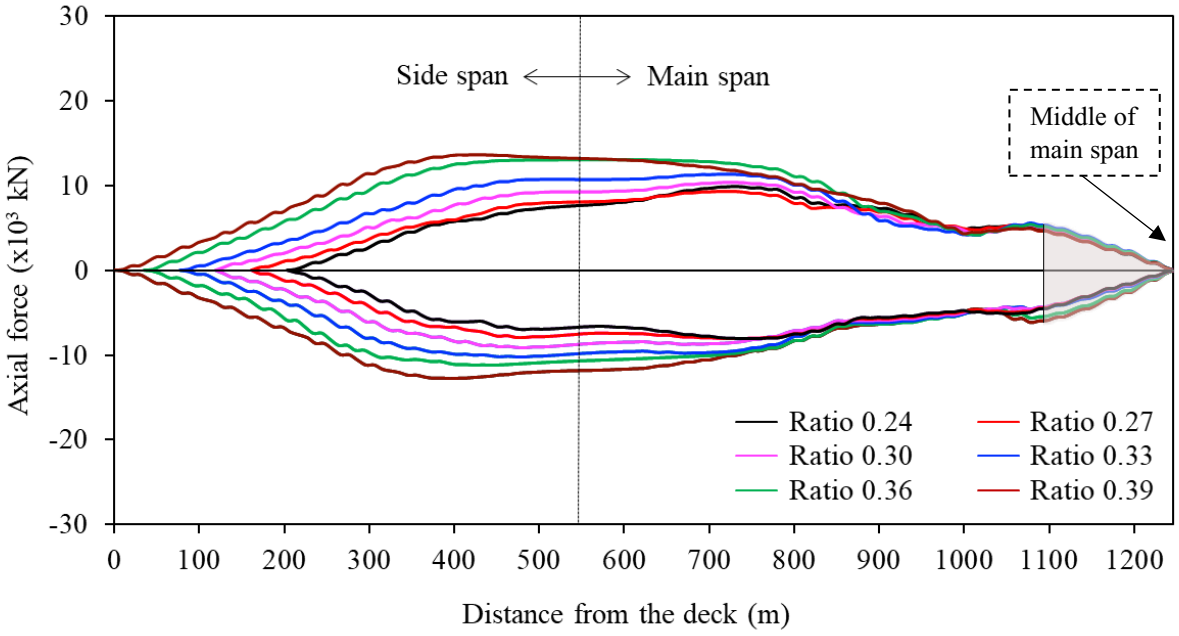

Figure 4.7 Maximum tensile and compressive force in the girder due to EQ.

Bending moment

Figure 4.8 presents the bending moment envelopes corresponding to EQ for the side-to-main span ratios of 0.24, 0.33, and 0.39. The shape of three envelopes is the same while the amplitude of the moment varies. It can be seen in Fig. 4.8, for the ratios of 0.24 and 0.33, the maximum bending moment in the girder under EQ occurs near the middle of the main span where crossing cables are installed. However, for the ratio of 0.39, the maximum bending moment is observed in the side span, this finding is consistent with the observation from the static load analysis as discussed in previous section. Furthermore, it can be found in Fig. 4.8, with the increase of the side-to-main span ratio the bending moment at the main span decreases dramatically while the bending moment at the side span changes slightly.

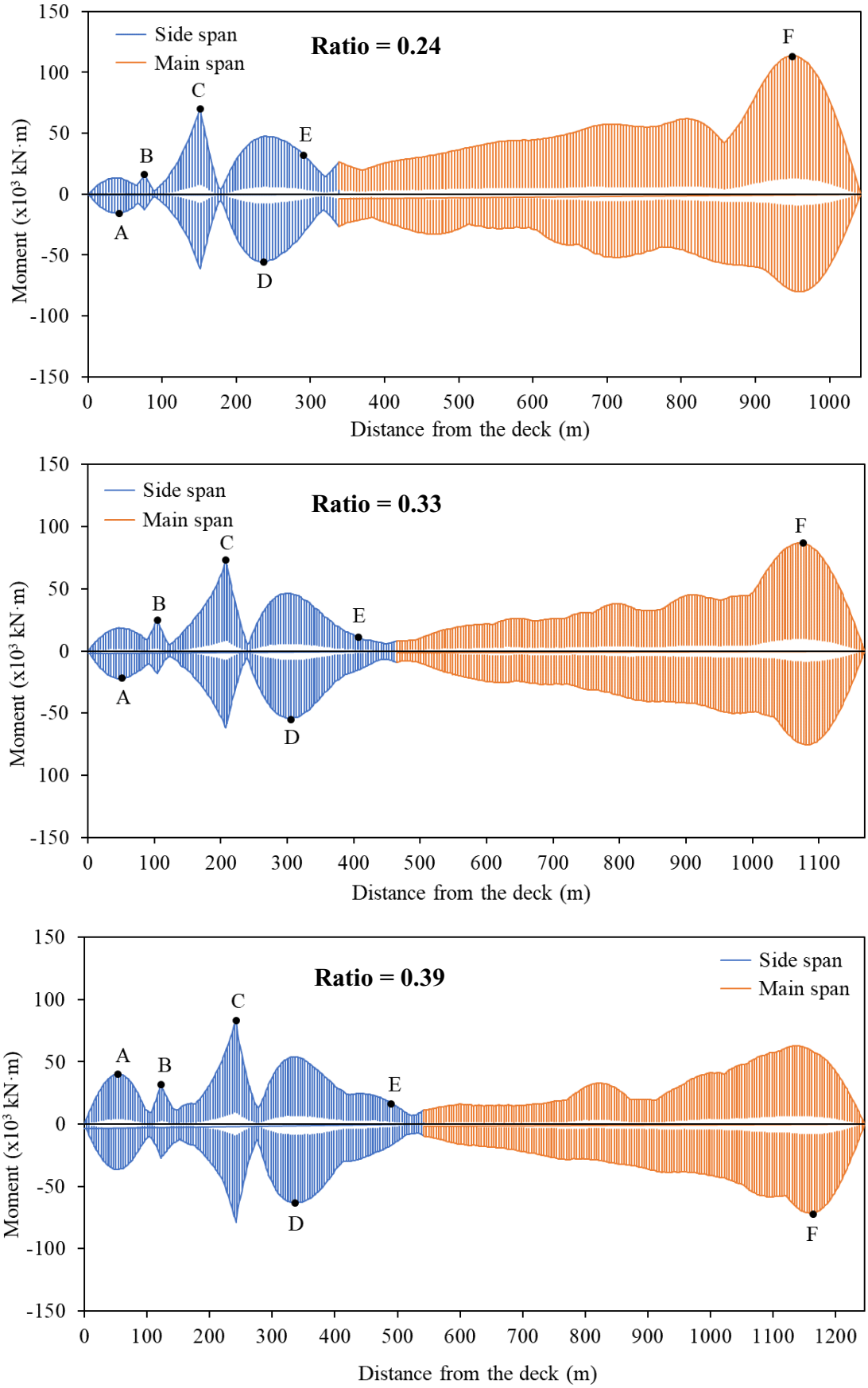

Figure 4.8 Moment envelope due to (EQ) for the ratios 0.24, 0.33 and 0.39.

Table 4.10 shows the maximum absolute moments at 6 typical points along the girder for the 6 ratios examined. It is found that the maximum moment among these points, which is located at point F (middle of the main span), for the ratio of 0.24 is about 1.6 times the amount for the ratio of 0.39. Given relatively larger moment induced near the middle of the main span, attention needs to be given to the earthquake response for side-to-main span ratios of 0.24, 0.27, and 0.30.

Table 4.10 Maximum absolute moment (kN·m) in the girder at selected nodes due to EQ.

Point*	Side-to-main span ratio						Ratio of max. to min.
	0.24	0.27	0.30	0.33	0.36	0.39	
A	16	14	17	22	32	40	2.86
B	16	17	17	25	29	32	2.00
C	70	63	67	73	79	83	1.32
D	56	49	50	54	64	63	1.31
E	32	23	18	11	17	15	2.91
F	113	106	95	87	74	71	1.59

*Location of each point is defined in Table 4.3.

Stress

Table 4.11 lists the maximum compressive and tensile stresses due to EQ. Based on the above discussion on the seismic response of axial force and bending moment, it is expected that larger stress be observed for the side-to-main span ratio of 0.24 while smaller stress for the ratio of 0.39 as given in the table. In addition, compressive stress and tensile stress are quite close for the 6 ratios tested except for the ratio of 0.36, the variation between the two stresses is about 3MPa.

Table 4.11 Maximum compressive and tensile stress in the girder due to EQ.

Side-to-main span ratio	Compressive stress (MPa)	Tensile stress (MPa)
0.24	-43.8	44.1
0.27	-40.8	41.3
0.30	-36.7	37.7
0.33	-32.7	34.3
0.36	-32.3	29.4
0.39	-34.9	32.9
Average	**-36.9**	**36.6**

Deflection

It is known that excessive longitudinal movement could cause severe damage to bridges during earthquake events especially for bridges with a fully floating system (Liu et al., 2008). Recently, Hariri and Lin (2018) reported that cable-stayed bridges would be vulnerable to vertical displacement subjected to seismic excitations. Given this, both horizontal and vertical displacements of the bridge were examined. Figure 4.9a presents time histories of the longitudinal displacement of a joint on the girder aligned with Pylon 1 for all the six side-to-main span ratios. Figure 4.9b shows the girder vertical displacement time histories of a point around the middle of the main span where the maximum was observed. By comparing the two sets of the time histories, it can be seen that the peak of the vertical displacement arrives after the horizontal. This is due to the fact that the vibration of the bridge is dominated by the motion in the horizontal direction as discussed in Section 3.4.2, Chapter 3. In addition, results from this study show that the vertical deck displacement is larger than the horizontal displacement as much as about three times (Table 4.12), which is consistent with the finding reported in Hariri and Lin (2018). Furthermore, it can be seen in the figure that the residual vertical displacement is much larger than the horizontal one. Thus, members sensitive to vertical

ground motions might suffer from major damage during severe earthquake events. The displacement results in Table 4.12 demonstrate that the deck longitudinal displacement is the same for all six cases. The results for the vertical displacement can be divided into two groups, one for the ratios of 0.24, 0.27, 0.30 and 0.33, and the other for ratios of 0.36 and 0.39. The difference between these two groups is about 13%, which is not significant.

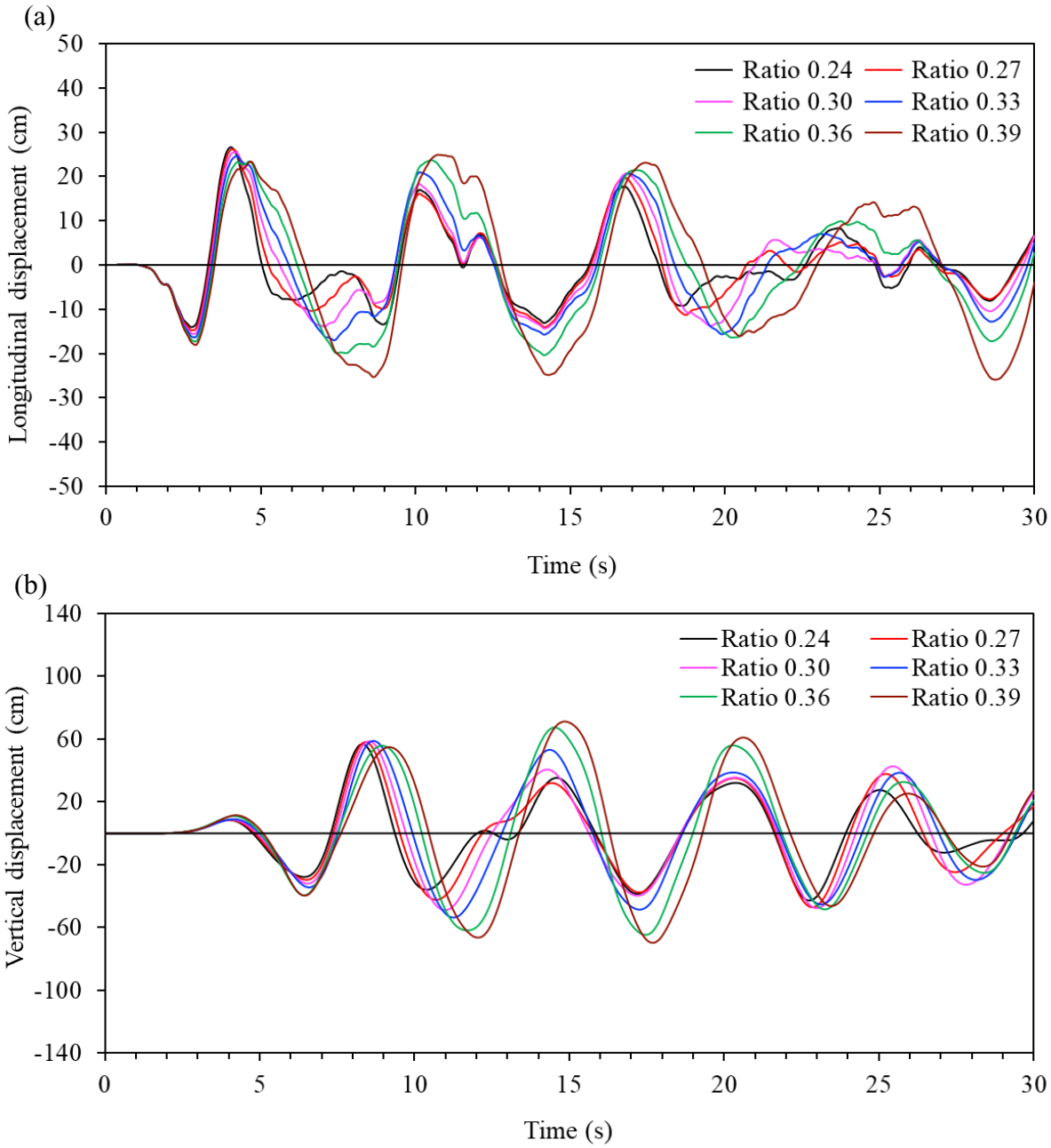

Figure 4.9 Displacement time history: (a) longitudinal displacement; (b) vertical displacement

Table 4.12 Maximum deck longitudinal and vertical displacement due to EQ.

Side-to-main span ratio	Longitudinal displacement (cm)	Vertical displacement (cm)
0.24	27	57
0.27	26	58
0.30	26	59
0.33	25	59
0.36	24	67
0.39	26	71

4.3.2 Cable force

The force in each cable group generated by EQ is presented in Table 4.13. It should be noted that the cable groups in the table are the same as those considered in the static analysis. The results in Table 4.12 show that the side-to-main span ratio of 0.39 developed the largest cable forces among the 6 ratios examined except: (i) group C5 where the ratio of 0.33 geneartes the largest foce, and (ii) group C9 where the ratio 0.24 provides the largest. Furthermore, there is no significant difference on the froce for group C11 for all the cases considered. As presented in Table 4.12, the ratio of the maximum to minimum response from the 6 ratios ranges from 1.05 (Group C11) to 1.92 (Group C1-C4). It is important to mention that the cable force due to EQ is much less than that due to traffic load. Therefore, the effect of EQ on the cable forces should not be a concern in the design and evaluation of cable-stayed bridges like the one considered in this study.

Table 4.13 Cable force (kN) due to earthquake load

Cable group ID	Side-to-main span ratio						Ratio of max. to min.
	0.24	0.27	0.30	0.33	0.36	0.39	
C1-C4	204	185	208	240	273	356	1.92
C5	300	290	305	315	275	285	1.15
C6	295	279	241	258	300	357	1.48
C7	298	247	273	305	392	446	1.81
C8	330	318	350	384	390	414	1.30
C9	385	332	320	318	303	300	1.28
C10	332	320	345	405	467	454	1.46
C11	174	170	172	168	174	177	1.05

4.3.3 Pylon

The response of pylon under EQ is investigated through the time history of the lateral displacement at the top of the pylon (Fig. 4.10) and the distribution of the bending moment along the height of the pylon (Fig. 4.11).

It can be seen in Fig. 4.10 that the wave form of the displacement time history of all cases is almost the same. The first peak arrives about 4.5s after the motion starts, then it comes back at about 10s mark. After these two peaks, the vibration of the pylon starts to decay which lasts about 15s. Finally, the pylon reaches the peak for a third time at about 2s before the motion stops, and the peak occurs in the opposite direction of the first one (5s mark). The residual displacement in the pylon is also quite significant. It was found in the study that the maximum lateral displacement given by all the six ratios is almost the same.

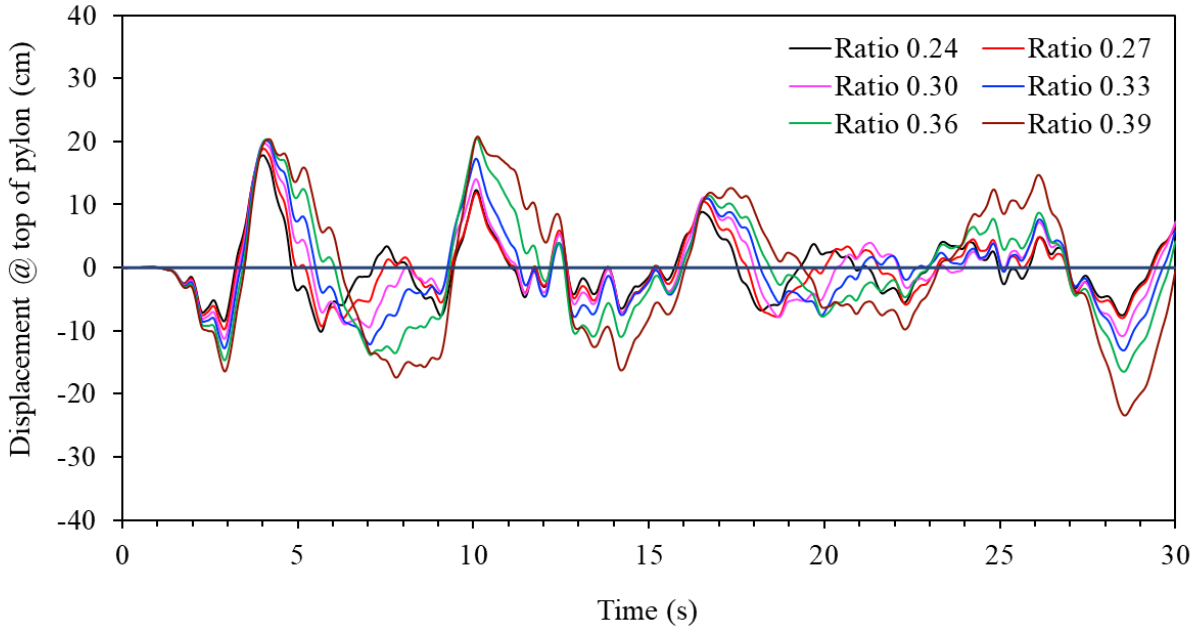

Figure 4.10 Pylon lateral top displacement time history.

With respect to the results of the moment in the pylon (Fig. 4.11), significant moment is expected at the bottom of the pylon since it is assumed to be fully fixed in the modelling. As illustrated in the figure, the other two critical sections with relatively larger moment are located at the center of the girder and at the intersection where the two pylon legs merge together (see Fig. 3.3, Chapter 3). Figure 4.11 clearly show that the six ratios generate the same moment distribution.

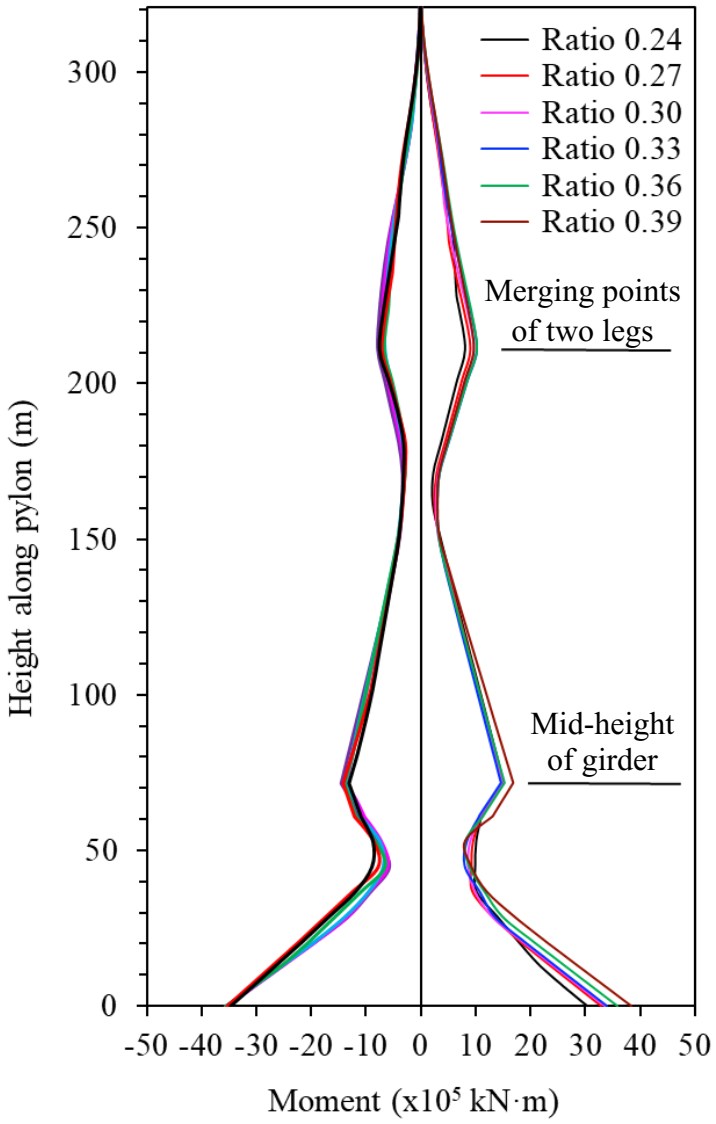

Figure 4.11 Moment distribution along height of pylon due to EQ.

4.3.4 Pier

The earthquake induced uplift force is presented in Table 4.14. As discussed in Section 4.3.1 (deflection), horizontal ground motion excitation causes the bridge to vibrate in the vertical direction, therefore, uplift force is generated at the side span in order to balance the vertical earthquake force at the main span. As seen in Table 4.13 earthquake load produces much larger uplift force in P2 (closer to Pylon 1) than in P1. In terms of the results for P1, the three smaller

ratios 0.24, 0.27 and 0.30 give almost the same force. It is observed in the table that the uplift force decreases from the ratio of 0.24 till 0.30, then it increases from the ratio of 0.33 to 0.39. It is important to mention that the uplift force developed by EQ is smaller than that by traffic load (see Table 4.9).

Table 4.14 Earthquake load induced uplift force (kN) in piers.

Item	Side-to-main span ratio					
	0.24	0.27	0.30	0.33	0.36	0.39
Force in P1	2210	2157	2200	2635	2852	2966
Force in P2	4929	4331	4241	4436	4762	5266
Ratio of force in P2 to P1	**2.23**	**2.00**	**1.93**	**1.68**	**1.67**	**1.78**

4.3.5 Anchorage force

The observation from the results of the anchorage force under EQ (Fig. 4.12) is the same as the one from the static analysis, i.e., the horizontal anchorage force is much larger the vertical force. It can be seen in Fig. 4.12 that the side-to-main span ratios of 0.24 and 0.39 induces relatively larger horizontal anchorage force compared with other ratios. For example, the anchorage force associated with the ratio of 0.24 is about 25% larger than that with the ratio of 0.36, which is not very significant considering the size of the bridge. The three ratios 0.27, 0.30, and 0.33 lead to almost the same horizontal force. In general, the anchorage force due to seismic load is much smaller compared with the force induced by dead load and traffic load (see Fig. 4.5).

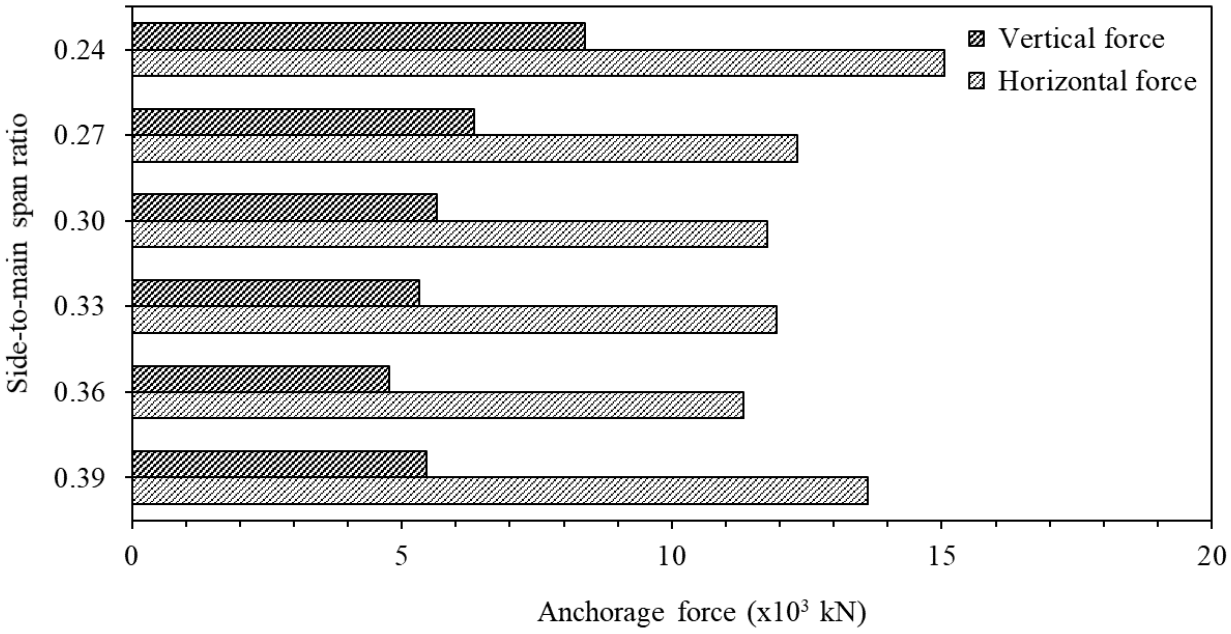

Figure 4.12 Vertical and horizontal components of anchorage force due to EQ.

CHAPTER 5

CONCLUSIONS

5.1 Introduction

The objective of this study is to evaluate behaviour of a cable-stayed bridge with a newly introduced anchorage system, namely, partially earth-anchored system with crossing cables, under different side-to-main span ratios. Given this, a bridge initially proposed by Shao et al. (2014) is selected to be examined in this study. This bridge has seven spans with a main span of 1408 m. The total steel deck width is about 42.4 m, and it is continuous over all the seven spans. The pylons are A-shaped with a height of 321.1 m. Due to lack of information, cables are designed in accordance with Zero-displacement method described in Wang et al. (1993).

Structural analysis software SAP2000 is used to develop a three-dimensional finite element model of the bridge in question. The dynamic characteristics of the modal developed in this study is compared with those provided in Shao et al. (2014) in terms of modal frequencies and mode shapes. Since a good matching is observed in comparison, the model developed is used for further analysis.

In this study, six side-to-main span ratios 0.24, 0.27, 0.30, 0.33, 0.36 and 0.39 are considered to examine the bridge performance. The parameters selected for this investigation cover the response of both superstructure and substructure, such as, girders, cables, pylons and piers. Forces to be used for the design of anchorage zones are also considered in the examination. Two typical loads, i.e., static loads and dynamic load, are applied on the bridge model. The static loads are represented by dead load and traffic load while dynamic load is represented by earthquake load.

5.2 Conclusions

The major conclusions drawn from this study with respect to ***static loads*** are summarized as follows:

(1) Girder:

- The effectiveness and efficiency of crossing cables is noticeable for larger side-to-main span ratio (referred as span ratio hereafter) in reducing the significant tensile force developed in the main span.
- The span ratio does not affect the moment at the main span. It has major effects on the side span in the region close to the anchorage block.
- The maximum compressive stress in the girder at the side and main spans is the same for each span ratio examined. However, it is not the case for the tensile stress.
- Deck vibration and the movement in the longitudinal direction due to traffic load should not be a concern.

(2) Cable: The difference on the cable force between different span ratios is less than 10%. Thus, the span ratio has very minor effect on the force in cables.

(3) Pylon: Both bending moment and lateral displacement change linearly with the span ratio.

(4) Pier: The span ratio has more effect on the uplift force in the pier far away from the pylon. The uplift force in the pier close to the pylon is almost the same.

(5) Anchorage force: Smaller span ratio leads to larger anchorage force. The anchorage force provides by the ratio of 0.24 is about 80% larger than that by the ratio of 0.39.

With respect to the dynamic load examined in the study, it can be concluded that earthquake load is not a concern in the design and evaluation of the super long bridges like the one

considered in the study. However, attention should be paid to the following response parameters,

(1) Longitudinal deck displacement to have sufficient seat width.

(2) Residual displacement of the deck in both longitudinal and vertical direction to avoid severe damage to the deck during earthquake events. .

5.3 Recommendations for Future Work

Partially earth-anchored system with crossing cables is a very unique system proposed a few years ago with an intention to expand the main span length. Given the development of the new system at its early stage, some additional work would be beneficial, for example,

1. Perform ambient vibration test in order to validate the finite element model for structural analysis.

2. Conduct seismic analysis on the bridge model using multi-support excitation. The decay of both time and amplitude of the shear wave traveling from one pylon to another could not be ignored in this case. This is because the main span is super long.

3. Investigate bridge performance under wind load by carrying out both wind tunnel tests and numerical analysis. The bridge is most likely sensitive to wind load than earthquake load.

References

Bittner, R.B., Safaqah, O., Zhang, X., and Jensen, O.J. (2007). Design and construction of the Sutong Bridge foundations. The Journal of the Deep Foundations Institute, **1**(1): 2-18. DOI: 10.1179/dfi.2007.001

Chen, D.W., Au, F.T.K., Tham, L.G., and Lee, P.K.K. (2000). Determination of initial cable forces in prestressed concrete cable-stayed bridges for a given design deck profiles using the force equilibrium method. Journal of Computers and Structures, **74**(1): 1-9.

Cid, C., Baldomir, A., and Hernández, S. (2018). Optimum crossing cable system in multi span cable-stayed bridges. Engineering Structures, Vol: 160, pp. 342-355. DOI:10.1016/j.eng Struct.2018.01.019.

CSA-S6-14. (2014). Canadian Highway Bridge Design Code (CHBDC). Canadian Standard Association, Ottawa, Ont.

CSI (2018). SAP2000 Integrated Software for Structural Analysis and Design, V20.1.0, Computers and Structures Inc., Berkeley, California.

Gimsing, N.J. (1988). Cable-stayed bridges with ultra-long spans, Lyngby, Denmark.

Gimsing, N.J., and Georgakis, C.T. (2012). Cable Supported Bridges: Concept and Design, Third Edition, John Wiley & Sons, Ltd, Chichester, United Kingdom.

Hassan, M.M., Nassef, A.O., and El Damatty, A.A. (2013). Optimal design of semi-fan cable-stayed bridges. Canadian Journal of Civil Engineering, NRC research press, **40**(3): 285-297. DOI:10.1139/cjce-2012-0032

Hariri, B., and Lin, L. (2018). Evaluating the response of cable-stayed bridges subjected to delayed seismic time-histories using multi-support excitation. Proceedings of the 3rd International Conference on Civil, Structural and Transportation Engineering (ICCSTE'18) Niagara Falls, Canada, June 10-12, 2018. Paper No. 145:1-8. DOI:10.11159/iccste18.145.

Janjic, D., Pircher, M., and Pircher, H. (2003). Optimization of cable tensioning in cable-stayed bridges. Journal of Bridge Engineering, **8**(3): 131-137. DOI:10.1061/(ASCE)1084-0702(2003)8: 3(131).

Jin, Z., Pei, S., Wei, X., Liu, H., and Qiang, S. (2016). Partially earth-anchored cable bridge: Ultralong-span system suitable for carbon-fiber-reinforced plastic cables. Journal of Bridge Engineering, **21**(6): 06016003. DOI:10.1061/(ASCE)BE.1943-5592.0000877.

Kim, S., and Won, J. (2016). Structural behaviour of a long-span partially earth-anchored cable-stayed bridge during installation of a key segment by thermal prestressing. Applied Sciences Journal, **6**(8): 231. DOI:10.3390/app6080231.

Leonhardt, F. (1987). Special Report: Cable Stayed Bridges with Prestressed Concrete. PCI Journal, **32**(5): 52-80.

Liu, J.L., Li, H., and Ou, J.P. (2008). Investigation of seismic performance of cable-stayed bridges with different connections. Proceedings of the 14th World Conference on Earthquake Engineering, Beijing, China, 12-17 October 2008. Paper ID: 14_06-0170.

Muller, J. (1992). The bi-stayed bridge concept: Overview of wind engineering problems. Proceedings of the first International Symposium on Aerodynamics of Large Bridges, Copenhagen, Denmark, February 19-21, 1992. pp. 237-245.

Nagai, M., Fujino, Y., Yamaguchi, H., and Iwasaki, E. (2004). Feasibility of a 1,400m span steel cable-stayed bridge. Journal of Bridge Engineering, **9**(5): 444–452. DOI:10.1061/(ASCE)1084-0702(2004)9:5(444).

Negrão, J.H.O., and Simões, L.M.C. (1997). Optimization of cable-stayed bridges with three-dimensional modelling. Journal of Computers & Structures, **64**(1-4): 741-58.

Otsuka, H., Tanaka, H., Noguchi, J., Etoh, T., and Sakai, I. (1990). Partially anchored composite cable-stayed bridge, IABSE Symposium Report, Brussels, pp. 347-351.

Shao, X., Hu, J., Deng, L., and Cao, J. (2014). Conceptual design of superspan partial ground-anchored cable-stayed bridge with crossing stay cables. Journal of Bridge Engineering, **19**(3): 1-5. DOI:10.1061/(ASCE)BE.1943-5592.0000534.

Shao, Y., Shao, X., Li, Li., and Wu, J. (2017). Optimum combination of bridge and deck systems for superspan cable-stayed bridges. Journal of Bridge Engineering, **23**(1): 1-11. DOI:10.1061/(ASCE)BE.1943-5592.0001161.

Simões, L.M.C., and Negrão, J.H.O. (2000). Optimization of cable-stayed bridges with box girder decks. Journal of Advances in Engineering Software, **31**(6): 417-423. DOI: 10.1016/0965-9978(00)00003-X.

Starossek, U. (1996). Cable-stayed bridge concept for longer spans. Journal of Bridge Engineering, **1**(3): 99-103.

Sun, B., Cheng, J., and Xiao, R.C. (2010). Preliminary design and parametric study of 1400 m partially earth-anchored cable-stayed bridge. Science China Technological Sciences, **53**(2): 502-511. DOI:10.1007/s11431-010-0041-4.

Svensson, H. (2012). Cable-Stayed Bridges: 40 Years of Experience Worldwide, First Edition, Ernst & Sohn GmbH & Co.KG., Berlin, Germany.

Tang, M. (2000). Cable-stayed bridges. Bridge Engineering Handbook. *Edited by* Chen, W. and Duan, L. CRC Press LLC, Florida, USA, Chapter 19, pp. 19.1-19.17.

Wang, Y.C., Vlahinos, A.S., and Shu, H.S. (1997). Optimization of cable preloading on cable-stayed bridges. Proceedings of SPIE 3043, Smart Structures and Materials 1997: Smart Systems for Bridges, Structures, and Highways, May 23rd, 1997. pp. 248-259.

Wang, P.H., Tseng, T.C., and Yang, C.G. (1993). Initial shape of cable-stayed bridges with three-dimensional modelling. Journal of Computers & Structures, **46**(6): 1095-1106.

Wilson, J., and Liu, T. (1991). Ambient vibration measurements on a cable-stayed bridge. Earthquake Engineering and Structural Dynamics, **20**(8): 723-747. DOI:10.1016/0045-7949(93)90284-K

Won, J. H., and Yoon, J.H. (2008). Structural effects of partially earth anchored cable system on medium-span cable-stayed bridges. Steel Structures, **8**(3): 225-236.

Zhang, X., Yuan, H., Pei, M., Dai, J., and Xu, L. (2009). General design of Sutong Bridge. Journal of Engineering Sciences, **7**(1): 6-11.